Journal of Medicinal Chemistry

pubs.acs.org/jmc

Article

LC-MF-4, a Novel FGFR3 Degrader for Therapeutic Intervention in FGFR3-Altered Cancers

Lulu Zheng,‖ Jiaqi Cao,‖ Lin Ma,‖ Shiyan Chen,‖ Xiansheng Cao, Ruixiang Luo, Yuhan Wang, Di Ke,* Ping Huang,* Guang Liang,* and Lingfeng Chen*

Cite This: J. Med. Chem. 2025, 68, 13858−13871

Read Online

ACCESS | Metrics & More | Article Recommendations | Supporting Information

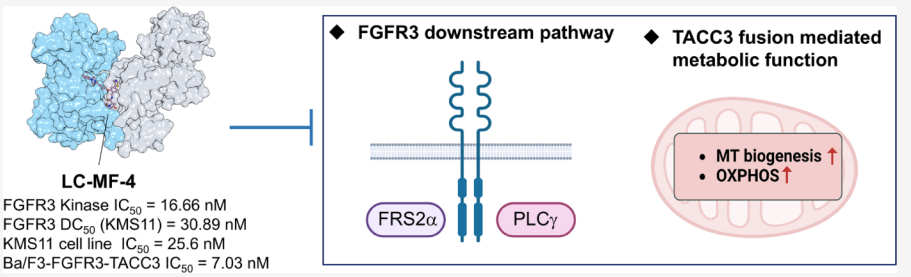

ABSTRACT: Alterations in the fibroblast growth factor receptor 3 (FGFR3) gene have been noted in human diseases, including bladder cancer and urothelial carcinoma (UC). Erdafitinib was approved for the treatment of UC but is limited by the progression of on-target gatekeeper resistance mutations. Several heterobifunctional FGFR degraders have been developed as potential therapeutic agents to block FGFR1 or FGFR2 signaling. However, to date, none of the FGFR3-active degraders have been identified. Herein, we report the discovery of LC-MF-4, the first efficient FGFR3 degrader, for the treatment of cancers harboring FGFR3 alterations. Proteomic analysis revealed that LC-MF-4 exhibits exceptional proteomic selectivity for FGFR3 degradation. In FGFR3-TACC3 fusion-positive cells, LC-MF-4 exerted its effects by suppressing the expression of genes involved in mitochondrial biogenesis and ATP synthesis. This study demonstrated robust antitumor activity of LC-MF-4 in the Ba/F3-FGFR3-TACC3 xenograft model, highlighting its potential for the treatment of FGFR3-altered cancers.

1. INTRODUCTION

Fibroblast growth factor receptors (FGFR1−4) are single transmembrane receptor tyrosine kinases (RTKs) that contains an extracellular ligand-binding domain (D1−D3), a short transmembrane domain, and a conserved intracellular kinase domain.[1,2] The FGFRs recognize paracrine and endocrine FGFs to mediate cell proliferation, differentiation, and metabolism homeostasis.[3] A-loop tyrosine transphosphorylation in the kinase domain of FGFR1−4 is achieved via ligand induced receptor dimerization, primarily triggered by FGF. Following kinase activation, FGFR recruit two direct substrates: FGFR substrate 2 alpha (FRS2a) and Phospholipase C gamma 1 (PLCγ), thereby activating multiple cascade pathways, including PI3K-AKT, MAPK-ERK, and STAT-dependent signaling.[2,4−7]

FGFR3 is a highly conserved member among four FGFRs, and the gene alterations in FGFR3, including amplifications, point mutations, or fusions, leads to oncogenesis.[8,9] Next-generation sequencing demonstrated that FGFR3 gene alteration has been identified in 80% of nonmuscle invasive bladder cancers and was detected in ∼20% of muscle invasive bladder cancers and urothelial carcinoma (UC).[10,11] Point mutations in the FGFR3 result in FGF independent receptor activation. We previously showed that a distinct pathogenic R669G gain-of-function mutation in FGFR3 kinase, promotes the formation of an asymmetric dimer by eliminating the repulsive force between two kinase domains.[8] Additionally, high frequency of the oncogenic gene fusion FGFR3-TACC3 was detected in UC and human glioblastoma. Transforming acidic coiled-coil containing protein 3 (TACC3) contains a coiled-coil domain, thus facilitating constitutive FGFR3 kinase transphosphorylation and relocalization.[7,12] Phosphopeptide PIN4 is a novel substrate of FGFR3-TACC3, which mediates the activation of mitochondrial metabolism and tumor growth.[13]

Erdafitinib is the only FDA-approved inhibitor for the treatment of patients with locally advanced UC harboring FGFR3 alterations,[14] while other pan-FGFR inhibitors infigratinib, futibatinib and pemigatinib were approved for the treatment of cholangiocarcinoma.[15,16] In adult patients

Received: March 12, 2025
Revised: June 16, 2025
Accepted: June 17, 2025
Published: June 27, 2025

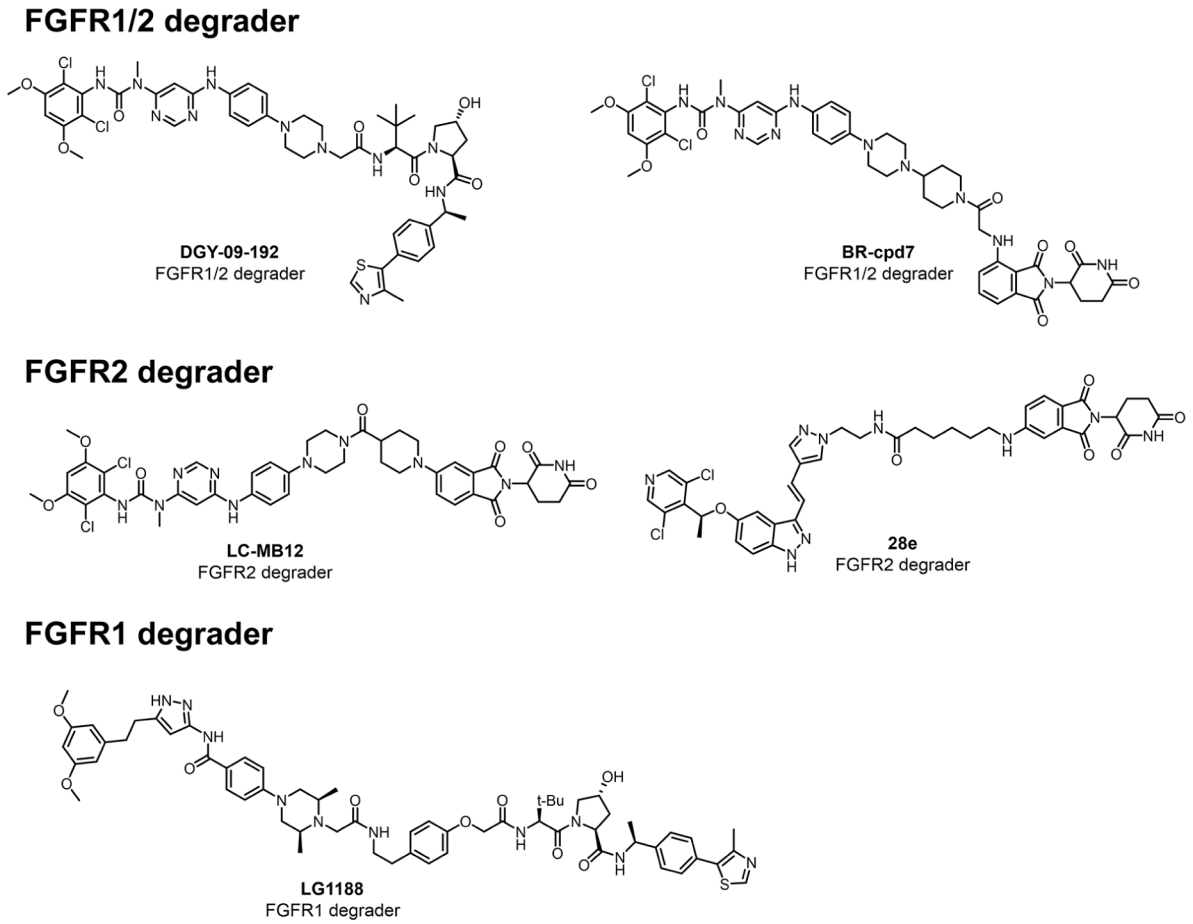

Figure 1. Chemical structure of reported FGFR1/2 degraders.

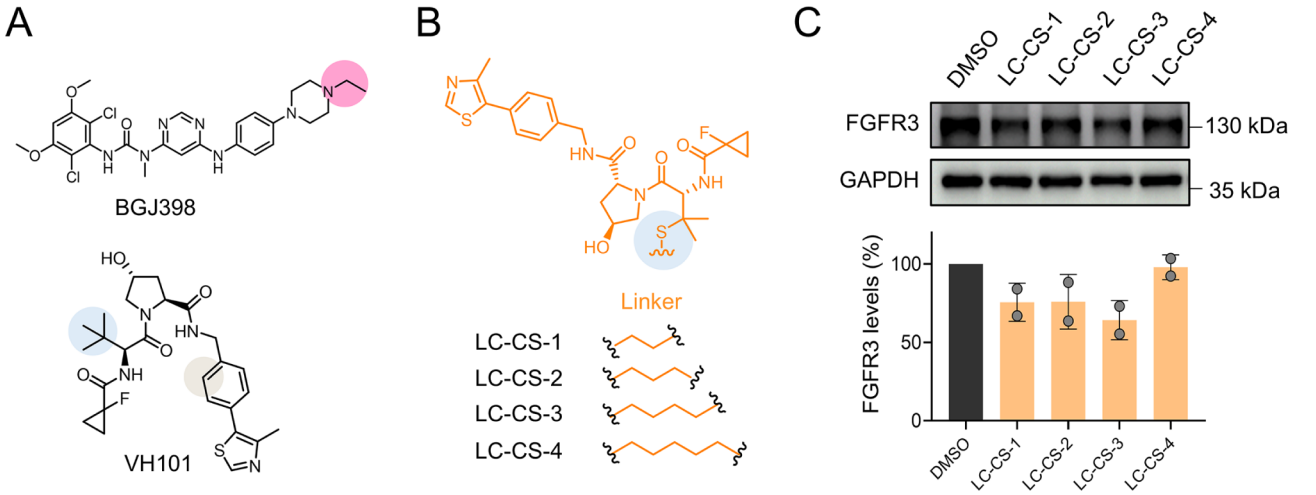

Figure 2. Degrader LC-CS-1 to LC-CS-4 screening. (A) Chemical structure of BGJ398 and VH101. (B) Structures of compounds LC-CS-1 to LC-CS-4. (C) Representative Western blots evaluating total FGFR3 levels in KMS-11 cells following 8 h of treatment with 100 nM of tested compounds or DMSO.

with locally advanced or metastatic UC that harboring FGFR3 alterations, erdafitinib administration significantly improved outcomes compared to chemotherapy, with a median overall survival of one year, an overall response rate of 35% and a median progression free survival of 5.6 months.[17] While these four approved pan-FGFR inhibitors provided clinical benefits, the long-term efficacy of these approved inhibitors has been hindered by the on-target acquired resistance.[18−20] Facchinetti et al. detected a high frequency of FGFR3 single or multiple mutations responsible for resistance to erdafitinib in 21 patients with UC.[21]

Proteolysis-targeting chimera (PROTAC) offers an effective alternative drug modality to overcome critical issues in cancer treatment, including insufficient efficacy and resistance.[22,23] Unlike classical inhibitors that block the catalytic function of the target protein, PROTACs remove the entire target protein.

https://doi.org/10.1021/acs.jmedchem.5c00731
J. Med. Chem. 2025, 68, 13858−13871

Scheme 1. Reaction Conditions: (a) i-PrOH, DIEA, 40 °C; (b) 1-Butanol, DIEA, Methylamine, 120 °C; (c) Toluene, DIEA, 80 °C; (d) DCM, TFA, r.t. (e) DCM, HATU, Et_3N, r.t.; (f) DCM, HCl·EA (2 M), r.t.; (g) DMF, HATU, Et_3N, 0 °C; (h) DCM, Piperidine, r.t.; (i) DMF, HATU, Et_3N, r.t.; (j) DCM, TFA, Triisopropylsilane, 0 °C; (k) DMF, K_2CO_3, 80 °C; (l) THF, HCl, 45 °C; (m) DCE/DMSO, $NaBH(OAc)_3$, Et_3N, r.t

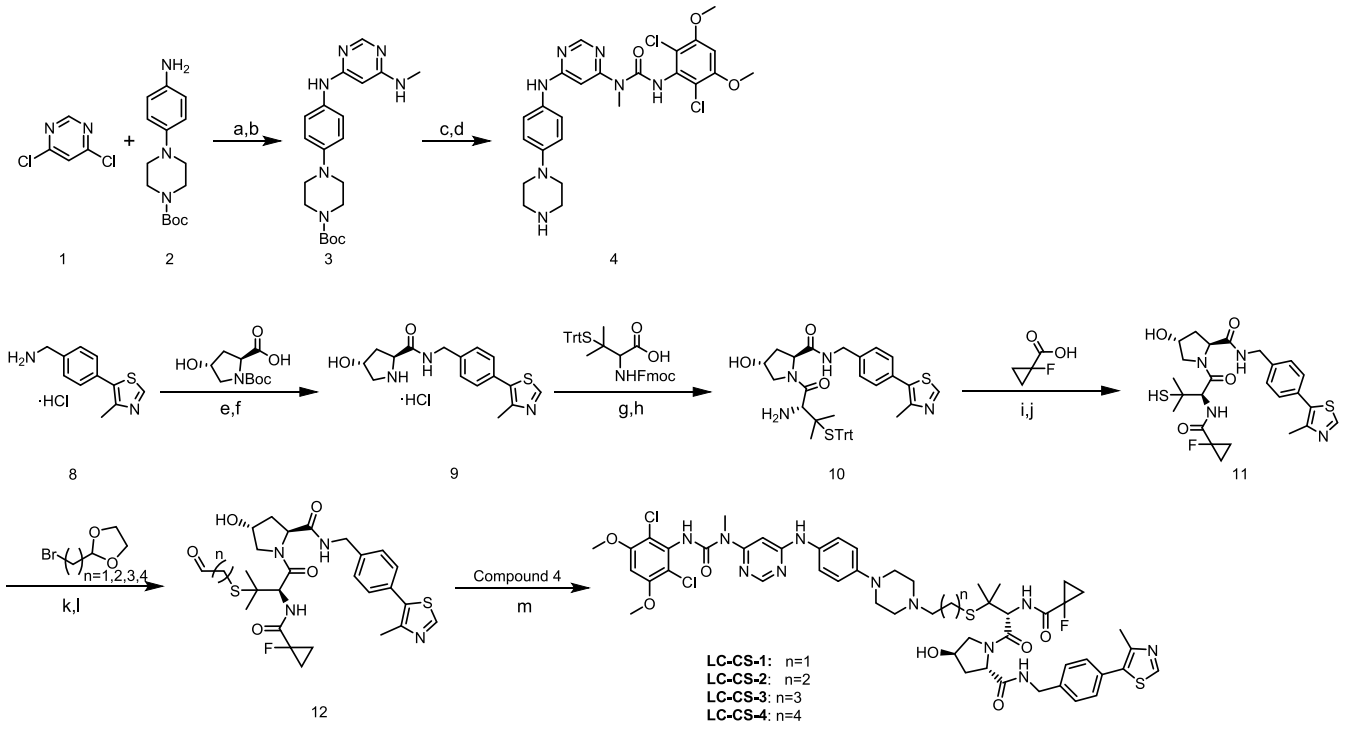

Scheme 2. Reaction Conditions: (a) DMF, K_2CO_3, 80 °C; (b) THF, HCl, 45 °C; (c) DCE/DMSO, $NaBH(OAc)_3$, Et_3N, r.t. (d) Acetone, K_2CO_3, 50 °C; (e) DMF, K_2CO_3, 80 °C

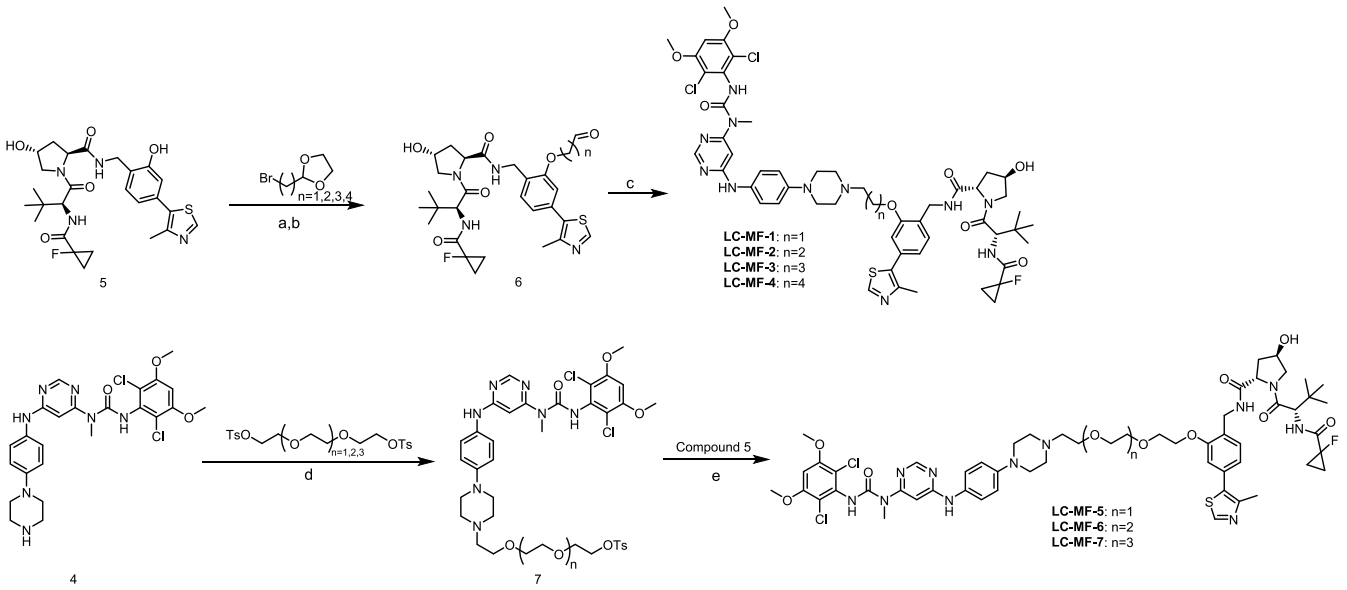

This indicates that there is a low risk of undesired on-target resistance or gain-of-function activity. Notably, PROTAC molecules can effectively remove fusion partners of the target, such as TACC3. Currently, more than 30 degraders have entered clinical trials for various indications, mainly cancer and autoimmune diseases.[24]

Since 2021, several FGFR-targeting degraders have been discovered (Figure 1). Based on the warhead of pan-FGFR inhibitor infigratinib, Gray's lab reported that the first von Hippel-Lindau (VHL)-based FGFR degrader DGY-09-192, which was identified as the potent dual degrader of FGFR1 and 2, fails to degrade FGFR3 and 4 isoforms.[25] In 2023, we discovered that a CRBN-based FGFR degrader LC-MB12, demonstrated potent degradation of FGFR2 *in vivo*, while showing less potency to FGFR1 and completely no degradation activity against FGFR3.[26] Similar results were observed for other reported FGFR1 or FGFR2 degraders incorporated with different pan-FGFR targeting warheads

https://doi.org/10.1021/acs.jmedchem.5c00731
J. Med. Chem. 2025, 68, 13858−13871

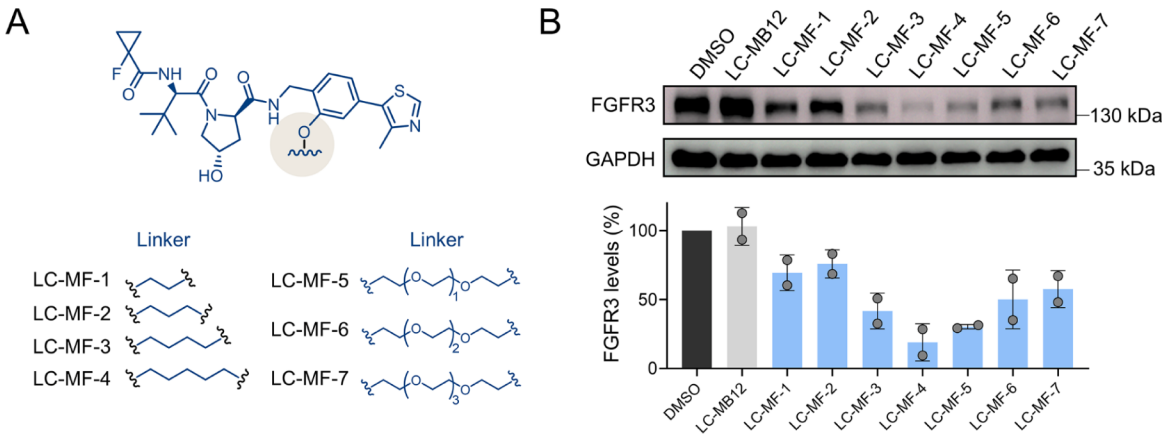

Figure 3. Degrader LC-MF-1 to LC-MF-7 screening. (A) Structures of compounds LC-MF-1 to LC-MF-7. (B) Representative Western blots evaluating total FGFR3 levels in KMS-11 cells following 8 h of treatment with 100 nM of tested compounds.

(Figure 1).[27−30] Therefore, FGFR3 isoform-active degraders remain unavailable. Herein, we report that the development and characterization of LC-MF-4, the first efficient FGFR3 degrader LC-MF-4 for the treatment of cancers harboring FGFR3 mutations or FGFR3-TACC3 alterations.

2. RESULTS AND DISCUSSION

2.1. Development of Initial VH101 Thioether-Linked Degraders as Moderate FGFR3 Degraders. The sequence composition of the FGFR3 catalytic binding site is highly conserved among human FGFRs, and the development of FGFR3 isoform-selective warheads has been unsuccessful. Thus, we initiated a study using infigratinib as an FGFR3 inhibitor due to its potency and selectivity against FGFR. The piperazine ring of infigratinib was exposed to the solvent, providing a suitable exit vector for linker attachment (Figure 2A). For E3 ubiquitin ligases, we recruited VHL101 because the CRBN-based degraders developed in our previous study failed to induce FGFR3 degradation (Figure 2A).[26]

First, the intermediates of infigratinib and VH101 with the exit vector positioned outside the *tert*-leucine site, were synthesized and tethered together via alkyl-based linkers (Scheme 1), generating four initial compounds, LC-CS-1 to LC-CS-4 (Figure 2B). Human myeloma KMS-11 cells, which endogenously express appreciable levels of FGFR3, were used for bifunctional molecular evaluation by Western blotting. KMS-11 cells were treated with the compounds at 100 nM for 8 h, and the level of FGFR3 was determined (Figure 2C). The results indicated that all four compounds harboring the thioether-linked VHL ligand showed only modest degradation potency against FGFR3 at 100 nM concentration, resulting in the degradation of 5−35% of FGFR3. This suggests an unfavorable ternary complex formation between FGFR3 and thioether conjugated VHL. Therefore, we performed medicinal chemistry optimization with the goal to improve the compounds' effectiveness as FGFR3 degraders.

2.2. Identification of LC-MF-4 as Selective FGFR3 Degrader. Linker length and composition can remarkably affect the formation of the FGFR3-degrader-E3 ligase ternary complex. In pursuit of more efficient degraders that can result in the rapid degradation of FGFR3, we switched the attachment site of VHL101 from the *tert*-leucine site to the phenolic position, achieved by optimizing the synthetic route (Scheme 2), resulting in the compounds LC-MF-1 to LC-MF-7.

As shown in Figure 3, LC-MF-4 was the most effective optimized compound, degrading 82% of FGFR3 at 100 nM/8 h treatment. In contrast, degraders with shorter alkyl linkers (LC-MF-1 to LC-MF-3) or PEG-based linkers (LC-MF-5 to LC-MF-7) induced less degradation of FGFR3 under the same treatment conditions, which reduced FGFR3 levels by 24−69% relative to the vehicle control-treated cells at 8 h after treatment. The CRBN-based FGFR degrader, LC-MB12, showed no degradation activity against FGFR3.[26] On the basis of the analysis of the Western blots in KMS-11 cells, compound LC-MF-4 stood out as the most potent degrader of FGFR3 and was selected for further evaluation.

To characterize LC-MF-4, we performed a dose-dependent degradation assay (Figure 4A). LC-MF-4 showed potent degradation of FGFR3 following 8 h treatment (DC_{50} = 30.8 nM, D_{max} = 85%). The weak "hook effect" was observed at high concentrations above 3000 nM. In contrast, LC-CS-4, with the same linker as LC-MF-4, but different VHL-attaching sites, showed no FGFR3 degradation activity (Figure 4B,C). In addition, we analyzed FGFR3 levels by immunofluorescence assay, demonstrating that LC-MF-4 remarkably reduced the amount of FGFR3 after 6 or 12 h of treatment at 100 nM. To verify whether the difference in FGFR3 degradation activity between the LC-MF-4 and LC-CS-4 cells was due to their different affinities for FGFR3, we performed an in vitro FGFR3 kinase assay. Notably, both LC-MF-4 and LC-CS-4 showed high FGFR3 kinase inhibition potencies, with IC_{50} value of 16.6 and 11.3 nM, respectively (Figure 4E).

To assess the degradation selectivity of LC-MF-4, the global proteomic profile of LC-MF-4 in KMS-11 cells was examined (Figure 4F). To capture potential off-target proteins, KMS-11 cells were treated with the heterobifunctional molecule, LC-MF-4 at a high concentration of 500 nM for 8 h. Proteomic data showed that FGFR3 was the only protein that was significantly downregulated following LC-MF-4 treatment among the 6,643 proteins identified, indicating the high selectivity of LC-MF-4 across the proteome. Further cell-based experimental tests revealed that the LC-MF-4 exhibited degradation activity against both FGFR1 and FGFR2, while showing no detectable effect on FGFR4 (Figure S1).

2.3. LC-MF-4 Mediates Ternary Complex Formation. Both LC-MF-4 and LC-CS-4 showed comparable biochemical inhibition of FGFR3, but displayed different degradation

https://doi.org/10.1021/acs.jmedchem.5c00731
J. Med. Chem. 2025, 68, 13858−13871

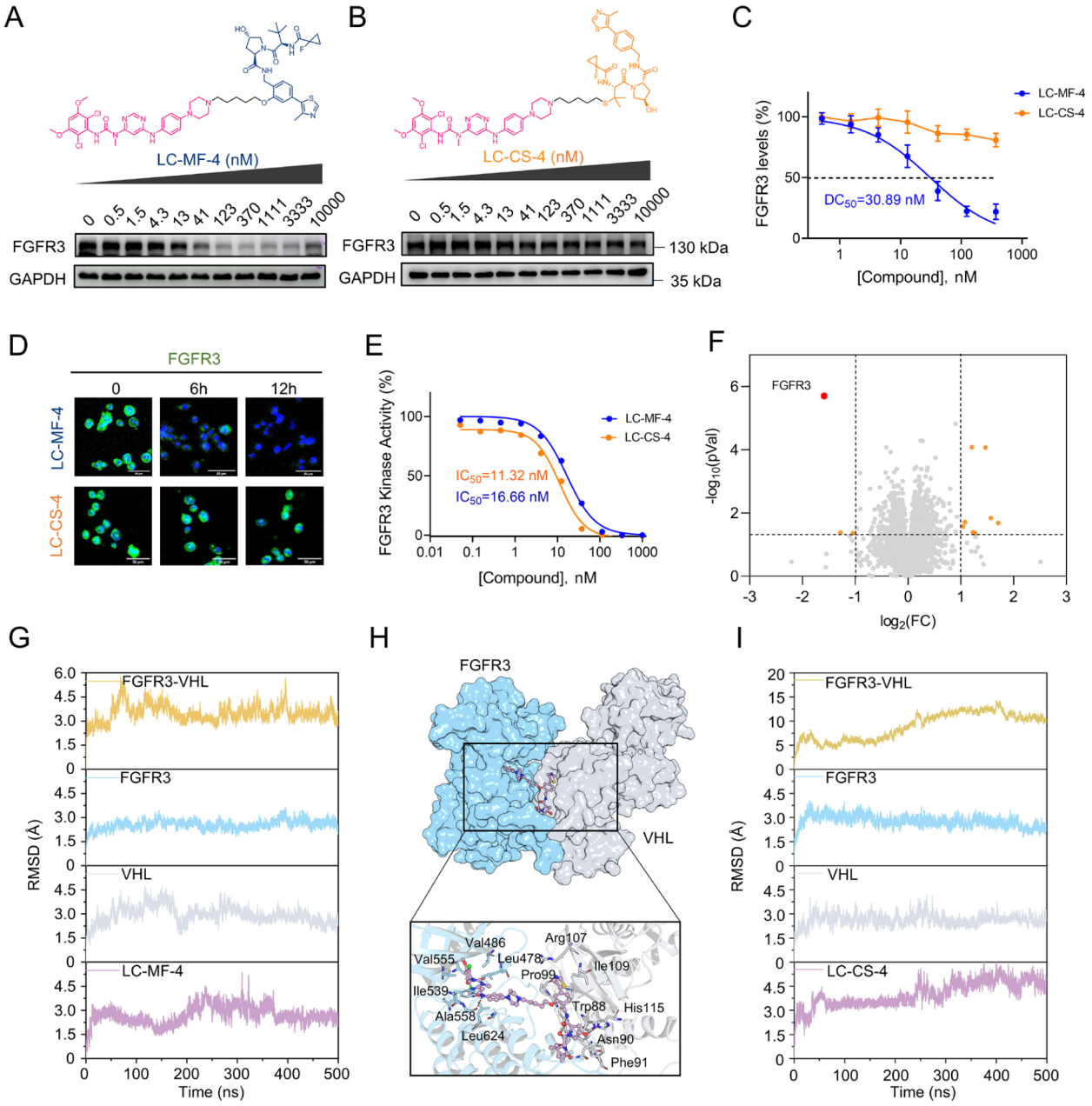

Figure 4. Identification of LC-MF-4 as an efficient FGFR3 degrader. (A−C) FGFR3 levels in KMS-11 cells after treatment with increasing concentrations of LC-MF-4 (A) or LC-CS-4 (B) for 8 h. Data were obtained from three biologically independent experiments. The DC_{50} value were shown (C). (D) Immunofluorescence images of FGFR3 (green) in KMS-11 cells after treatment with LC-MF-4 or LC-CS-4 for 0, 6, or 12 h. (E) The inhibitory activity of LC-MF-4 and LC-CS-4 against FGFR3 kinase domain. Data were obtained from two biologically independent experiments. (F) Global proteomics analysis. KMS-11 cells were treated with 500 nM LC-MF-4 for 8 h before proteomics measurement. (G) RMSD curves for FGFR3-VHL complex, FGFR3, VHL, and LC-MF-4 during 500 ns MD simulations. (H) Molecular modeling of the FGFR3-VHL-LC-MF-4 ternary complex. (I) RMSD curves for FGFR3-VHL complex, FGFR3, VHL, and LC-CS-4 during 500 ns MD simulations.

potencies (Figure 4E), indicating that the stability of the binary complex does not necessarily induce the formation of the ternary complex and target degradation. The *PROTAC-Model* method and molecular dynamics (MD) simulations were used to further investigate the dynamic behavior of ternary complex formation. This approach aimed to elucidate the binding mechanism and provide insights into LC-MF-4.[31] Initially, the *PROTAC-Model* method was used to construct the static ternary complex, followed by 500 ns MD simulations. The root-mean square deviations (RMSDs) of the protein backbone atoms (C_α) in the FGFR3-VHL complex, FGFR3, and VHL converged after approximately 200 ns, 80 ns, and 200 ns of MD simulations, respectively (Figure 4G). The RMSDs of LC-MF-4's heavy atoms stabilized after ∼370 ns. These results indicated that the ternary complex achieved stability after ∼370 ns of MD simulation and was robustly formed. To identify the key residues involved in the binding of LC-MF-4 to FGFR3 and VHL, per-residue contribution decomposition was performed using the mechanics/generalized Born surface area (MM/GBSA) method. The top 10 residues contributing to LC-MF-4 binding to FGFR3 were Ala558, Leu624, Val555, Leu478, Tyr557, Val486, Ile539, Gly561, Pro573, and Ala506 (Figures 4H and S2A,B). The key residues for VHL binding are Trp88, Pro99, Tyr98, Ile109, Arg107, His115, Gln96, Phe91,

https://doi.org/10.1021/acs.jmedchem.5c00731
J. Med. Chem. 2025, 68, 13858−13871

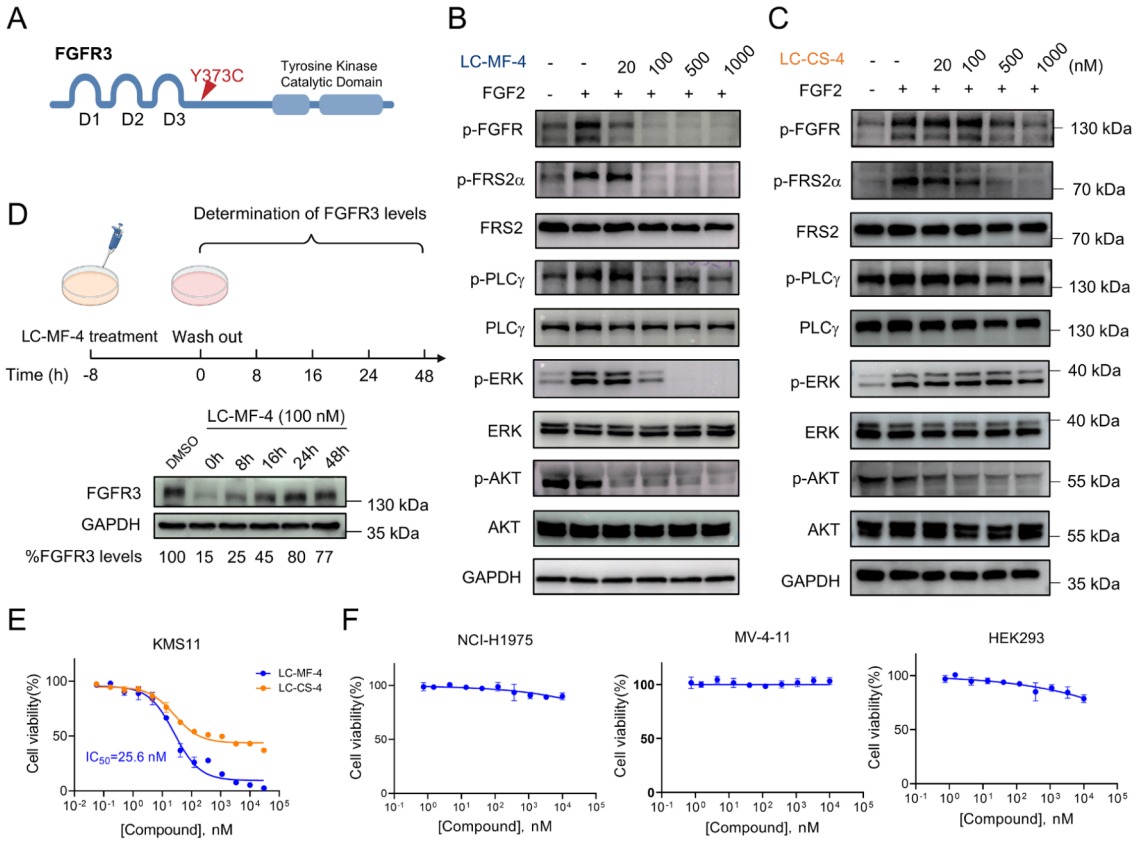

Figure 5. LC-MF-4 demonstrated a therapeutic effect in FGFR3 Y373C mutated cancer. (A) Schematic diagram of FGFR3 Y373C mutation. (B-C) The levels of p-FGFR, p-FRS2α, p-PLCγ, p-ERK, and p-AKT in KMS-11 cells after treatment with increasing concentrations of LC-MF-4 (B) or LC-CS-4 (C) for 8 h, followed by incubation with FGF2 for 10 min. (D) KMS-11 cells were treated with 100 nM LC-MF-4 for 8 h and then washed out. FGFR3 expression was measured at different time points (0, 8, 16, 24, and 48 h). (E) Proliferation assay of LC-MF-4 or LC-CS-4 on KMS-11 cells. (F) Proliferation assay of LC-MF-4 on NCI-H1975, MV-4−11, and HEK293 cells.

Asn90, and Pro86. Structural analysis revealed that LC-MF-4 formed hydrogen bonds with the hinge region of FGFR3 and with Tyr98 and His115 in VHL).

In comparison, LC-CS-4 failed to degrade FGFR3, although it had a low IC_{50} value (11.32 nM). Molecular modeling was used to investigate the underlying mechanisms. The FGFR3-VHL complex did not achieve stable convergence during the 500 ns of MD simulations, even though FGFR3, VHL, and LC-CS-4 individually stabilized within 50 ns (Figure 4I). This suggests that the FGFR3-VHL-LC-CS-4 ternary complex did not form a stable configuration. Alignment of the final snapshots of FGFR3-VHL-LC-MF-4 (light blue) and FGFR3-VHL-LC-CS-4 (gray) revealed that the VHL-binding positions differed significantly (Figure S2C,D). Additionally, MM/GBSA-based binding free energy calculations showed that the binding energy of LC-MF-4 to FGFR3-VHL was −83.87 kcal/mol, whereas LC-CS-4 had a binding energy of −59.29 kcal/mol. These findings support the conclusion that LC-MF-4 forms a more stable ternary complex with FGFR3 and VHL than LC-CS-4.

2.4. LC-MF-4 Demonstrated Therapeutic Effects in FGFR3 Y373C Mutated Cancer. One of the most common FGFR3 alterations is the Y373C point mutation in the transmembrane region of receptor found in bladder cancer and UC.[32] FGFR3 Y373C oncogenic variant generates an unpaired cysteine residue between the extracellular D2 and D3 domains, resulting in ligand-independent FGFR3 dimerization (Figure 5A). We assessed the functional consequences of LC-MF-4 induced degradation compared to that of the control molecule, LC-CS-4 (an active FGFR3 kinase inhibitor that failed to mediate degradation), in KMS-11 cells harboring the Y373C mutation. Robust FGFR3 A-loop tyrosine (Tyr647/648) and downstream phosphorylation of FRS2α and PLCγ were observed in KMS-11 cells (Figure 5B). Upon paracrine ligand stimulation, the A-loop phosphorylation of FGFR3 was stimulated, which was completely blocked by LC-MF-4 at the concentration of 100 nM. In addition, cells treated with LC-MF-4 exhibited significantly lower phosphorylation of receptors and downstream substrates than those treated with LC-CS-4 (Figure 5C). RNA sequencing analysis determined that the degradation of the FGFR3 protein led to the inhibition of gene expression related to cancers and cytokine-cytokine receptor interaction (Figure S3). Those result was consistent with the ability of LC-MF-4 to induce FGFR3 degradation, thereby enhancing the suppression of downstream signaling activation.

To verify the capacity of LC-MF-4 for FGFR3 degradation, we assessed sustained cellular degradative potency through washout experiments (Figure 5D). In KMS-11 cells, FGFR3 protein levels were reduced to 10% after 8 h of treatment with 100 nM LC-MF-4, and maintained at <50% for 16 h after LC-MF-4 removal. These findings suggest that FGFR3 has a relatively slow turnover in KMS-11 cells and that LC-MF-4 induces a long-lasting effect on the depletion of FGFR3, implying the potential for reduced dosing frequency in clinical regimens.

https://doi.org/10.1021/acs.jmedchem.5c00731
J. Med. Chem. 2025, 68, 13858−13871

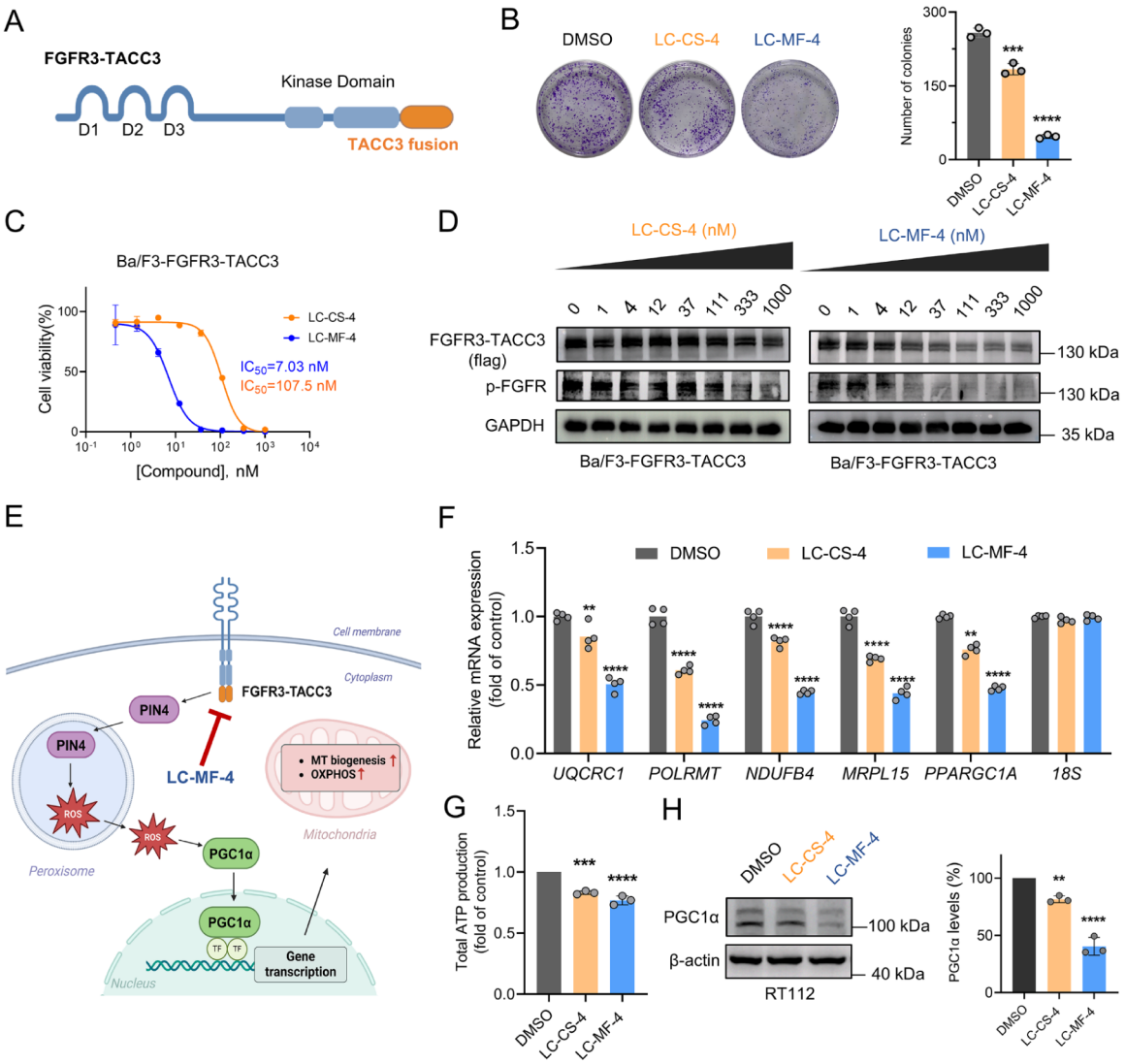

Figure 6. LC-MF-4 inhibits the metabolic function of FGFR3-TACC3 fusion positive cancer. (A) Schematic diagram of the FGFR3-TACC3 fusion protein. (B) Colony formation assay of RT112 cells treated with 100 nM LC-CS-4, LC-MF-4, or DMSO. (C) Proliferation assay of LC-MF-4 or LC-CS-4 in Ba/F3-FGFR3-TACC3 cells. (D) TH phosphorylated and total level of FGFR3-TACC3 in Ba/F3-FGFR3-TACC3 cells treated with increasing concentrations of LC-CS-4 or LC-MF-4. (E) Schematic diagram of mitochondrial metabolism affected by FGFR3-TACC3 fusion. (F) Relative RNA expression of genes involved in mitochondrial function (*UQCRC1*, *POLRMT*, *NDUFB4*, *MRPL15*, and *PPARGC1α*) in RT112 cells treated with 100 nM LC-CS-4, LC-MF-4, or DMSO for 8 h ($n = 4$). (G) Total ATP production in RT112 cells treated with 100 nM LC-CS-4, LC-MF-4, or DMSO for 8 h ($n = 3$). (H) PGC1α expression in RT112 cells treated with 100 nM LC-CS-4, LC-MF-4, or DMSO for 8 h ($n = 3$). One-way ANOVA with Dunnett's post hoc test for multiple comparisons of differences in the means of DMSO, LC-MF-4-treated, and LC-CS-4-treated groups. mean ± SD $^*p < 0.05$, $^{**}p < 0.01$, $^{***}p < 0.001$, and $^{****}p < 0.0001$.

We examined the antiproliferative effects of LC-MF-4 on KMS-11 cells. LC-MF-4 efficiently inhibited cell proliferation driven by FGFR3 Y373C, with an antiproliferative IC_{50} of 25.6 nM after 72 h of treatment (Figure 5E,F). In contrast, LC-CS-4 exhibited 17-fold lower potency in the proliferation assay. Notably, LC-MF-4 did not inhibit the growth of HEK293T cells with low FGFR3 expression, or cancer cell lines driven by EGFR, FLT3- ITD.

2.5. LC-MF-4 Inhibits the Metabolic Function of FGFR3-TACC3 Fusion Positive Cancer. Constitutive activation of FGFR3 can be driven by its fusion with TACC3, which promotes ligand-independent dimerization and enhances mitochondrial metabolism in cancer cells (Figure 6A).[13,33] We explored the effect of LC-MF-4 on the growth of RT112 bladder cells expressing the FGFR3-TACC3 fusion protein.[34] LC-MF-4 significantly inhibits the colony formation and proliferation in FGFR3 fusion-positive cell line (Figures 6B and S4). In addition, LC-MF-4 dramatically inhibited the proliferation of engineered Ba/F3 cells expressing FGFR3-TACC3 with an IC_{50} of 7.03 nM (Figure 6C), which was 15-fold more potent than that of the FGFR3 kinase inhibitor LC-CS-4 (107.5 nM). To distinguish differences in potency, Ba/F3-FGFR3-TACC3 cells were treated with two representative heterobifunctional molecules at a wide range of concentrations (Figure 6D). These results suggested that LC-MF-4 induced a dose-dependent reduction in oncogenic FGFR3-TACC3 protein levels, in line with the decrease in A-loop tyrosine phosphorylation induced by the TACC3 fusion partner.

FGFR3-TACC3 has been reported to signal via PIN4, causing vesicle trafficking, that results in the accumulation of ROS, elevated mitochondrial metabolism, and increased ATP synthesis (Figure 6E).[13] We assessed whether direct

https://doi.org/10.1021/acs.jmedchem.5c00731
J. Med. Chem. 2025, 68, 13858−13871

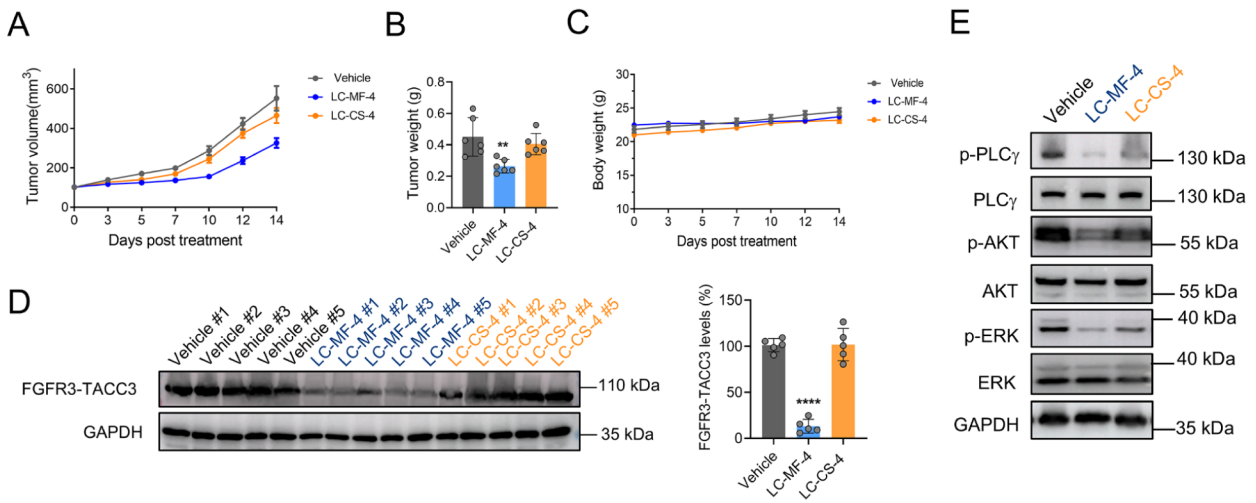

Figure 7. LC-MF-4 is a potent FGFR3 degrader *in vivo*. (A) Antitumor efficacy of LC-MF-4, LC-CS-4, or vehicle (20 mg/kg) in female BALB/c nude mice (n = 6) xenografted with Ba/F3-FGFR3-TACC3 cells. Tumor size was measured every 2−3 days after administration. (B) Tumor weight was assessed at the end of the treatment. (C) Body weight of nude mice during treatment. (D) The levels of FGFR3-TACC3 in tumor lysate. (E) Western blot evaluation of p-PLCγ, p-AKT, and p-ERK in tumor lysates. One-way ANOVA with Dunnett's post hoc test for multiple comparisons of differences in the means of Vehicle, LC-MF-4-treated, and LC-CS-4-treated groups. mean ± SD *p < 0.05, **p < 0.01, ***p < 0.001, and ****p < 0.0001.

degradation of the FGFR3-TACC3 fusion protein could more effectively interfere with TACC3-mediated functions than simply inhibiting FGFR3 kinase activity. The results showed that LC-MF-4 treatment significantly inhibited the expression of respiratory complex-related genes and mitochondrial RNA polymerase genes, such as *UQCRC1* and *POLRMT* in RT112 cells compared to DMSO or LC-CS-4 treated cells (Figure 6F). LC-MF-4 exerted its effects by decreasing ATP levels, as determined by ATP assays (Figure 6G). Elevated ROS levels stimulate the production of peroxisome proliferator-activated receptor gamma coactivator 1-alpha (PGC1a), a transcriptional coactivator encoded by *PARGC1A* and plays a central role in mitochondrial biogenesis and energy production.[35] Compound LC-MF-4 significantly inhibited the PGC1a protein expression and the *PARGC1A* mRNA level (Figure 6F,H). Taken together, these data indicate that LC-MF-4 regulates energy metabolism in RT112 cells by degrading FGFR3-TACC3.

2.6. LC-MF-4 Is Highly Effective in FGFR3-TACC3-Driven Tumor Models. To assess the drug development potential of LC-MF-4, we tested in vitro ADME profiling of LC-MF-4. The results showed high stabilities of LC-MF-4 in human liver microsomes with $T_{1/2}$ > 60 min (Table S1) and high plasma protein binding rate (98.9%) in human plasma (Table S2). Permeability measurements were performed for LC-MF-4 in Caco-2 cell line (Table S3). Due to high lipophilicity and molecular weight, LC-MF-4 showed high efflux ratio value. Additionally, we evaluated the potential inhibitory effect of LC-MF-4 on hERG in vitro. The results demonstrated that LC-MF-4 exhibited no hERG toxicity risk (IC_{50} > 30 μM, Figure S5). We next evaluated its pharmacokinetic (PK) properties in mice following oral administration and intravenous injection. LC-MF-4 showed rapid absorption, with plasma concentrations maintained above the DC_{50} values for LC-MF-4 during the experimental period (Table S4). To the best of our knowledge, this is the first report on a VHL-based FGFR degrader that is orally bioavailable with F = 4.07%.

Based on the *in vitro* experiments and pharmacokinetic analyses, we examined the *in vivo* efficacy of LC-MF-4 in Ba/F3-FGFR3-TACC3 cell-derived xenograft model. LC-MF-4 achieved 50.2% tumor growth inhibition in the BaF3-FGFR3-TACC3 xenograft model, whereas LC-CS-4 resulted in 19.3% tumor growth inhibition (Figure 7A,B). No significant body weight loss or adverse effects were observed in any group during the treatment (Figure 7C). Next, we evaluated the effects of LC-MF-4 on FGFR3-TACC3 and its downstream signaling in tumor tissues. The administration of LC-MF-4 resulted in a significant reduction in FGFR3-TACC3 protein levels (Figure 7D). Compared to LC-CS-4, LC-MF-4 showed superior inhibition of the phosphorylation levels of the downstream proteins PLCγ, AKT, and ERK1/2 (Figure 7E). These results indicate that LC-MF-4 is an effective degrader *in vivo*, making it a novel and promising candidate for the treatment of FGFR3-TACC3 fusion-positive tumors.

3. CONCLUSION

Alterations in FGFR3 act as oncogenes. The development of effective therapeutic strategies targeting FGFR3-altered cancers remains an urgent clinical need.[36] PROTAC technology has demonstrated promising potential as a protein degradation strategy, with notable advantages compared to traditional kinase inhibitors.[37] However, despite the development of several FGFR1/2 degraders, the discovery of FGFR3 degraders has been unsuccessful. In our study, we present LC-MF-4, the first potent FGFR3 degrader capable of eliminating FGFR3 in cancers harboring mutations or FGFR3-TACC3 fusions. LC-MF-4 demonstrated exceptional target selectivity, as evidenced by proteomic profiling, and achieved robust FGFR3 degradation in Y373C-mutated and FGFR3-TACC3 fusion-driven models. However, the current limitation of LC-MF-4 is lacks the ability to achieve selective degradation of the FGFR3 isoform. Recently, several compounds demonstrating selective targeting of FGFR3 have been reported, including TYRA-300 and LOXO-435.[17,38] In future studies, we intend to explore structure-based optimization strategies to improve FGFR3

https://doi.org/10.1021/acs.jmedchem.5c00731
J. Med. Chem. 2025, 68, 13858−13871

isoform target specificity, which we believe will further advance the therapeutic potential.

Unlike conventional inhibitors, LC-MF-4 ablates the FGFR3 kinase activity and removes the entire target protein at low nanomolar concentrations. This degradation-driven mechanism results in potent suppression of downstream signaling cascades and FGFR3-dependent proliferation. In addition, LC-MF-4 regulates mitochondrial metabolism mediated by FGFR3-TACC3 fusion, as evidenced by reduced ATP synthesis and inhibition of mitochondrial biogenesis genes. Molecular dynamics simulations further rationalized that LC-MF-4 induces stable ternary complex formation with FGFR3 and VHL, a feature absent in its nondegrading counterparts, such as LC-CS-4. Notably, LC-MF-4 exhibited *in vivo* efficacy in FGFR3-TACC3 xenograft models, achieving significant tumor growth inhibition with no significant toxicity.

In summary, LC-MF-4 represents a paradigm shift toward targeting FGFR3-driven malignancies. By leveraging the PROTAC technology to eliminate oncogenic FGFR3 entirely, this degrader broadly suppresses both kinase-dependent and noncatalytic oncogenic functions, such as fusion protein-mediated metabolic reprogramming. This degrader may also circumvent kinase-on-target resistance mechanisms through protein degradation. These findings suggest that LC-MF-4 is a promising candidate for FGFR3-altered cancers and underscores the therapeutic potential of selective degraders in precision oncology. Future studies should focus on optimizing pharmacokinetics and improve the FGFR3 isoform selectivity to maximize the clinical benefits.

4. EXPERIMENTAL SECTION

4.1. Chemistry. Commercial reagents, including solvents and other chemicals, were used as received without additional purification. All reagents were purchased from Sigma-Aldrich, Aladdin, and Energy Chemicals. All reactions were monitored using thin-layer chromatography (TLC). ^{1}H NMR and ^{13}C NMR) spectra were recorded on a Bruker 400 MHz instrument. Electrospray ionization mass spectra in positive mode (ESI-MS positive) were obtained by using an Agilent InfinityLab LC/MSD iQ (SG2233B005). Chromatographic purification was performed using Silica Gel 60. The purities of all the synthesized compounds were >95%, determined using the analytical HPLC on a Shimadzu LC-20AD system equipped with a UV detector (SPD-20A) and a Diamonsil C18 column (5 μm, 250 mm × 4.6 mm). The ^{1}H and ^{13}C NMR spectra of the synthesized compounds are presented.

*4.1.1. tert-Butyl 4-(4-((6-(methylamino)pyrimidin-4-yl)amino)-phenyl)piperazine-1-carboxylate (**3**).* Step 1. Compound **1** (2.98 g, 20 mmol) and compound **2** (5.55 g, 20 mmol) were dissolved in isopropanol (120 mL). Then, *N*,*N*-diisopropylethylamine (10.4 mL, 60 mmol) was added and the mixture was stirred at room temperature overnight. The reaction solution was filtered, and the solid product was washed with ethanol to afford the crude product as an off-white solid (6.4 g, 83%).

Step 2. Previous off-white product (6.4 g, 16.4 mmol) and 10 mL methylamine (30−33 wt.% in methanol) were dissolved in 1-butanol (60 mL). Then, *N*,*N*-diisopropylethylamine (8.4 mL, 49 mmol) was added and the mixture was stirred at 120 °C overnight. The solvent was evaporated and the residue purified by silica gel chromatography to provide the title compound as a white solid (5.61 g, 14.60 mmol, 89%).

*4.1.2. 3-(2,6-Dichloro-3,5-dimethoxyphenyl)-1-methyl-1-(6-((4-(piperazin-1-yl)phenyl)amino)pyrimidin-4-yl)urea (**4**).* Step 1. Compound **3** (384 mg, 1 mmol) and 2,4-dichloro-3-isocyanato-1,5-dimethoxybenzene (248 mg, 1 mmol) were dissolved in toluene (15 mL). Then, *N*,*N*-diisopropylethylamine (0.69 mL, 4 mmol) was added and the mixture was stirred at 80 °C overnight. The solvent was evaporated and the residue purified by silica gel chromatography (DCM/MeOH 150:1) to provide the product as a brown oil (372 mg, 0.59 mmol, 59%).

Step 2. Previous brown oil product (372 mg, 0.59 mmol) was dissolved in DCM (4 mL). Then, trifluoroacetic acid (3 mL) was added and the mixture was stirred at room temperature 2 h. The solvent was evaporated to provide the title compound as a white solid (307 mg, 0.58 mmol, 98%).

*4.1.3. (2S,4R)-1-((S)-2-(1-Fluorocyclopropane-1-carboxamido)-3,3-dimethylbutanoyl)-4-hydroxy-N-(4-(4-methylthiazol-5-yl)-2-(2-oxoethoxy)benzyl)pyrrolidine-2-carboxamide (**6a**).* Step 1. Compound **5** (120 mg, 0.22 mmol) and 2-bromo-1,1-diethoxyethane (66 mg, 0.33 mmol) were dissolved in DMF (2 mL). Then, K_2CO_3 (151 mg, 1.1 mmol) was added and the mixture was stirred at 80 °C for 3 h. The reaction mixture was diluted with water (30 mL), extracted with ethyl acetate (10 mL × 3), washed with brine (30 mL × 3). The combined organic layer was dried over anhydrous Na_2SO_4, filtered, and concentrated to dryness under reduced pressure to afford the crude product as a white oil (135 mg, 0.21 mmol, 95%).

Step 2. The white oil (135 mg, 0.21 mmol) was dissolved in THF (1.5 mL) and 0.5 M aq. HCl (1.5 mL). The reaction mixture was stirred at 70 °C for 1 h. The reaction was then concentrated to dryness under reduced pressure to give the title compound as a white oil (111 mg, 0.19 mmol, 92%).

*4.1.4. (2S,4R)-N-(2-(2-(4-(4-((6-(3-(2,6-Dichloro-3,5-dimethoxyphenyl)-1-methylureido)pyrimidin-4-yl)amino)phenyl)piperazin-1-yl)ethoxy)-4-(4-methylthiazol-5-yl)benzyl)-1-((S)-2-(1-fluorocyclopropane-1-carboxamido)-3,3-dimethylbutanoyl)-4-hydroxypyrrolidine-2-carboxamide (**LC-MF-1**).* Compound **4** (38 mg, 0.07 mmol) and compound **6a** (42 mg, 0.07 mmol) were added to DCE (2 mL), and then DMSO was added dropwise until complete dissolution. Et_3N (200 μL, 1.4 mmol) was then added followed by $NaBH(OAc)_3$ (60 mg, 0.28 mmol). The mixture was stirred at room temperature overnight. The reaction mixture was diluted with water (15 mL), extracted with DCM (5 mL × 3), washed with brine (20 mL × 3). The combined organic layer was dried over anhydrous Na_2SO_4, filtered, and concentrated to dryness under reduced pressure to afford the crude product. The residue purified by silica gel chromatography (DCM/MeOH 20:1) to provide the title compound as a white powder (33 mg, 0.03 mmol, 41%). ^{1}H NMR (400 MHz, Chloroform-*d*) δ 12.64 (s, 1H), 8.68 (s, 1H), 8.32 (s, 1H), 7.51 (t, J = 6.0 Hz, 1H), 7.47 (s, 1H), 7.36 (d, J = 7.7 Hz, 1H), 7.21 (d, J = 8.5 Hz, 2H), 7.09 (dd, J = 9.1, 3.6 Hz, 1H), 7.00−6.87 (m, 4H), 6.51 (s, 1H), 6.10 (s, 1H), 4.69 (t, J = 7.9 Hz, 1H), 4.60−4.39 (m, 4H), 4.21 (t, J = 5.6 Hz, 2H), 3.98−3.87 (m, 7H), 3.63 (dd, J = 11.2, 3.8 Hz, 1H), 3.29 (s, 3H), 3.29−3.21 (m, 4H), 3.01−2.91 (m, 2H), 2.85−2.78 (m, 4H), 2.52 (s, 3H), 2.48−2.34 (m, 1H), 2.13−2.01 (m, 1H), 1.40−1.18 (m, 4H), 0.94 (s, 9H). ^{13}C NMR (100 MHz, $CDCl_3$) δ 170.80, 170.72, 170.30, 170.10, 163.05, 160.64, 156.51, 155.84, 154.55, 153.43, 150.45, 149.20, 148.45, 135.02, 132.26, 131.75, 129.61, 129.47, 126.37, 125.14, 121.87, 116.91, 113.90, 112.17, 95.83, 87.13, 79.39, 77.40, 77.08, 76.76, 70.06, 65.96, 58.80, 57.41, 57.19, 56.72, 56.65, 53.55, 49.03, 38.90, 36.21, 35.59, 32.08, 29.71, 26.32, 16.16, 14.16, 13.74. LC−MS (ESI$^+$) m/z calcd for $C_{52}H_{63}Cl_2FN_{11}O_8S$ $[M + H]^+$, 1090.4, found 1090.4. HPLC t_R = 25.717 min (96.5% purity).

*4.1.5. (2S,4R)-N-(2-(3-(4-(4-((6-(3-(2,6-Dichloro-3,5-dimethoxyphenyl)-1-methylureido)pyrimidin-4-yl)amino)phenyl)piperazin-1-yl)propoxy)-4-(4-methylthiazol-5-yl)benzyl)-1-((S)-2-(1-fluorocyclopropane-1-carboxamido)-3,3-dimethylbutanoyl)-4-hydroxypyrrolidine-2-carboxamide (**LC-MF-2**).* **LC-MF-2** was synthesized in a similar manner as the bispecific compound **LC-MF-1**, white powder (39%). ^{1}H NMR (400 MHz, Chloroform-*d*) δ 12.66 (s, 1H), 8.33 (s, 1H), 7.56 (s, 1H), 7.26−7.19 (m, 2H), 7.01−6.92 (m, 2H), 6.51 (s, 1H), 6.11 (s, 1H), 3.91 (s, 6H), 3.75−3.59 (m, 1H), 3.30 (s, 3H), 3.28−3.21 (m, 4H), 2.83−2.76 (m, 1H), 2.69−2.61 (m, 4H), 2.57−2.45 (m, 2H), 1.87−1.75 (m, 1H), 1.44−1.15 (m, 15H). ^{13}C NMR (100 MHz, $CDCl_3$) δ 163.12, 160.68, 155.85, 154.54, 153.42, 149.32, 135.03, 129.32, 125.17, 116.82, 113.88, 95.77, 86.98, 77.40, 77.08, 76.77, 63.02, 58.90, 56.65, 56.60, 56.51, 53.20, 49.05, 35.36, 32.08, 31.95, 29.72, 29.47, 29.39, 27.23, 26.31, 25.78, 24.24, 22.72, 14.18.

https://doi.org/10.1021/acs.jmedchem.5c00731
J. Med. Chem. 2025, 68, 13858−13871

LC−MS (ESI$^+$) m/z calcd for $C_{53}H_{64}Cl_2FN_{11}O_8S$ [M + H]$^+$, 1104.4, found 1106.4. HPLC t_R = 25.740 min (94.85% purity).

*4.1.6. (2S,4R)-N-(2-(4-(4-(4-(((6-(3-(2,6-Dichloro-3,5-dimethoxyphenyl)-1-methylureido)pyrimidin-4-yl)amino)phenyl)piperazin-1-yl)butoxy)-4-(4-methylthiazol-5-yl)benzyl)-1-((S)-2-(1-fluorocyclopropane-1-carboxamido)-3,3-dimethylbutanoyl)-4-hydroxypyrrolidine-2-carboxamide (**LC-MF-3**).* **LC-MF-3** was synthesized in a similar manner as the bispecific compound **LC-MF-1**, white powder (43%). ^{1}H NMR (400 MHz, Chloroform-*d*) δ 12.66 (s, 1H), 8.67 (s, 1H), 8.32 (s, 1H), 7.62 (s, 1H), 7.42−7.31 (m, 2H), 7.26−7.18 (m, 2H), 7.11 (dd, J = 9.1, 3.6 Hz, 1H), 6.99−6.91 (m, 3H), 6.86 (d, J = 1.7 Hz, 1H), 6.51 (s, 1H), 6.10 (s, 1H), 4.72 (t, J = 7.7 Hz, 1H), 4.61−4.37 (m, 4H), 4.11−4.00 (m, 2H), 3.97−3.86 (m, 7H), 3.64 (dd, J = 8.2, 3.0 Hz, 1H), 3.29 (s, 3H), 3.27−3.20 (m, 4H), 2.70−2.63 (m, 4H), 2.54−2.43 (m, 6H), 2.14−2.01 (m, 1H), 1.96−1.85 (m, 2H), 1.83−1.71 (m, 2H), 1.40−1.26 (m, 4H), 0.94 (s, 9H). ^{13}C NMR (100 MHz, $CDCl_3$) δ 170.80, 170.74, 170.26, 170.06, 163.05, 160.62, 156.65, 155.82, 154.53, 153.45, 150.40, 149.18, 148.36, 135.00, 132.11, 131.89, 129.45, 129.31, 126.19, 125.07, 121.51, 116.83, 113.85, 111.94, 95.76, 87.08, 79.37, 77.43, 77.11, 76.79, 69.98, 67.84, 58.72, 58.15, 57.34, 56.64, 53.08, 48.93, 38.77, 36.08, 35.63, 32.08, 31.94, 31.60, 29.71, 29.38, 27.24, 26.30, 23.40, 22.72, 22.68, 16.14, 14.17, 13.75. LC−MS (ESI$^+$) m/z calcd for $C_{54}H_{66}Cl_2FN_{11}O_8S$ [M + H]$^+$, 1118.4, found 1118.5. HPLC t_R = 26.1 min (95.97% purity).

*4.1.7. (2S,4R)-N-(2-((5-(4-(4-(((6-(3-(2,6-Dichloro-3,5-dimethoxyphenyl)-1-methylureido)pyrimidin-4-yl)amino)phenyl)piperazin-1-yl)pentyl)oxy)-4-(4-methylthiazol-5-yl)benzyl)-1-((S)-2-(1-fluorocyclopropane-1-carboxamido)-3,3-dimethylbutanoyl)-4-hydroxypyrrolidine-2-carboxamide (**LC-MF-4**).* **LC-MF-4** was synthesized in a similar manner as the bispecific compound **LC-MF-1**, white powder (46%). ^{1}H NMR (400 MHz, Chloroform-*d*) δ 12.65 (s, 1H), 8.68 (s, 1H), 8.32 (s, 1H), 7.55 (s, 1H), 7.38−7.26 (m, 2H), 7.25−7.17 (m, 2H), 7.10 (dd, J = 9.0, 3.6 Hz, 1H), 6.98−6.91 (m, 3H), 6.85 (d, J = 1.7 Hz, 1H), 6.51 (s, 1H), 6.10 (s, 1H), 4.71 (t, J = 7.7 Hz, 1H), 4.61−4.37 (m, 4H), 4.07−3.97 (m, 2H), 3.98−3.86 (m, 7H), 3.64 (dd, J = 11.1, 4.0 Hz, 1H), 3.29 (s, 3H), 3.28−3.21 (m, 4H), 2.71−2.64 (m, 4H), 2.53−2.43 (m, 6H), 2.13−2.03 (m, 1H), 1.94−1.83 (m, 2H), 1.72−1.60 (m, 2H), 1.61−1.53 (m, 2H), 1.40−1.22 (m, 4H), 0.95 (s, 9H). ^{13}C NMR (100 MHz, $CDCl_3$) δ 170.82, 170.71, 170.27, 170.07, 163.06, 160.65, 156.70, 155.84, 154.55, 153.43, 150.36, 149.17, 148.38, 135.03, 132.12, 131.89, 129.49, 129.24, 126.21, 125.09, 121.48, 116.85, 113.91, 111.99, 95.84, 87.09, 79.38, 77.41, 77.09, 76.77, 70.01, 67.90, 58.71, 58.38, 57.36, 56.65, 56.56, 53.08, 48.90, 38.76, 36.09, 35.58, 32.08, 29.70, 29.15, 26.41, 26.30, 24.14, 16.13, 14.15, 13.74. LC−MS (ESI$^+$) m/z calcd for $C_{55}H_{68}Cl_2FN_{11}O_8S$ [M + H]$^+$, 1132.4, found 1132.3. HPLC t_R = 26.18 min (96.2% purity).

*4.1.8. 2-(2-(2-(4-(4-(((6-(3-(2,6-Dichloro-3,5-dimethoxyphenyl)-1-methylureido)pyrimidin-4-yl)amino)phenyl)piperazin-1-yl)ethoxy)-ethoxy)ethyl 4-methylbenzenesulfonate (compound **7a**).* Compound **4** (53.2 mg, 0.1 mmol) and (ethane-1,2-diylbis(oxy))bis-(ethane-2,1-diyl) bis(4-methylbenzenesulfonate) (138 mg, 0.3 mmol) were added to acetone (4 mL). K_2CO_3 was then added, and the reaction mixture was stirred at 50 °C overnight. The solvent was evaporated and the residue purified by silica gel chromatography (DCM/MeOH 50:1) to provide the title compound as a white oil (65 mg, 0.08 mmol, 80%).

*4.1.9. (2S,4R)-N-(2-(2-(2-(2-(4-(4-(((6-(3-(2,6-Dichloro-3,5-dimethoxyphenyl)-1-methylureido)pyrimidin-4-yl)amino)phenyl)-piperazin-1-yl)ethoxy)ethoxy)ethoxy)-4-(4-methylthiazol-5-yl)-benzyl)-1-((S)-2-(1-fluorocyclopropane-1-carboxamido)-3,3-dimethylbutanoyl)-4-hydroxypyrrolidine-2-carboxamide (**LC-MF-5**).* Compound **7a** (62 mg, 0.075 mmol) and compound **5** (40 mg, 0.075 mmol) were dissolved in DMF (2 mL). K_2CO_3 was then added, and the reaction mixture was stirred at 80 °C overnight. The reaction mixture was diluted with water (20 mL), extracted with DCM (5 mL × 3), washed with brine (30 mL × 3). The combined organic layer was dried over anhydrous Na_2SO_4, filtered, and concentrated to dryness under reduced pressure to afford the crude product. The residue purified by silica gel chromatography (DCM/MeOH 20:1) to provide the title compound as a white powder (26 mg, 0.022 mmol, 29%). ^{1}H NMR (400 MHz, Chloroform-*d*) δ 8.70 (s, 1H), 8.12 (s, 1H), 7.41−7.35 (m, 1H), 7.26−7.10 (m, 3H), 7.04−6.98 (m, 1H), 6.96−6.91 (m, 1H), 6.84 (d, J = 8.6 Hz, 2H), 6.54 (d, J = 11.6 Hz, 1H), 5.54 (s, 1H), 5.45 (s, 1H), 5.34 (s, 1H), 4.72−4.40 (m, 4H), 4.34−4.12 (m, 2H), 4.12−4.04 (m, 1H), 4.02−3.85 (m, 9H), 3.84−3.64 (m, 7H), 3.35−3.08 (m, 5H), 2.98−2.64 (m, 7H), 2.55 (s, 3H), 1.40−1.26 (m, 4H), 1.04−0.98 (m, 9H). ^{13}C NMR (100 MHz, $CDCl_3$) δ 170.87, 170.66, 170.27, 169.30, 169.10, 163.42, 163.11, 161.49, 160.75, 157.08, 156.90, 156.79, 155.95, 154.64, 154.60, 153.39, 153.02, 150.41, 149.02, 148.57, 148.54, 135.14, 133.33, 132.43, 132.31, 131.69, 130.50, 130.17, 129.86, 129.70, 127.15, 126.90, 125.20, 124.90, 122.32, 122.11, 117.03, 114.02, 113.28, 112.78, 96.27, 87.05, 79.51, 77.42, 77.10, 76.79, 74.32, 70.92, 70.79, 70.38, 70.08, 69.79, 69.69, 68.11, 68.02, 59.04, 58.91, 57.61, 57.48, 57.42, 57.31, 56.71, 56.66, 54.34, 53.39, 53.27, 48.66, 48.61, 39.42, 39.17, 36.76, 36.59, 35.76, 34.61, 32.13, 29.75, 28.42, 26.43, 16.22, 13.46, 13.36. LC−MS (ESI$^+$) m/z calcd for $C_{56}H_{70}Cl_2FN_{11}O_{10}S$ [M + H]$^+$, 1178.4, found 1178.5. HPLC t_R = 20.85 min (98% purity).

*4.1.10. (2S,4R)-N-(2-(2-(2-(2-(2-(4-(4-(((6-(3-(2,6-Dichloro-3,5-dimethoxyphenyl)-1-methylureido)pyrimidin-4-yl)amino)phenyl)-piperazin-1-yl)ethoxy)ethoxy)ethoxy)ethoxy)-4-(4-methylthiazol-5-yl)benzyl)-1-((S)-2-(1-fluorocyclopropane-1-carboxamido)-3,3-dimethylbutanoyl)-4-hydroxypyrrolidine-2-carboxamide (**LC-MF-6**).* **LC-MF-6** was synthesized in a similar manner as the bispecific compound **LC-MF-5**, white powder (31%). ^{1}H NMR (400 MHz, Chloroform-*d*) δ 8.71 (s, 1H), 8.13 (s, 1H), 7.47−7.34 (m, 1H), 7.27−7.11 (m, 3H), 7.04−6.86 (m, 4H), 6.55 (d, J = 8.0 Hz, 1H), 5.54 (s, 1H), 5.45 (s, 1H), 5.21 (s, 1H), 4.74−4.44 (m, 4H), 4.31−4.18 (m, 1H), 4.21−4.11 (m, 2H), 4.00−3.87 (m, 9H), 3.84−3.61 (m, 11H), 3.35−3.15 (m, 5H), 2.86−2.64 (m, 9H), 2.55 (s, 3H), 1.42−1.23 (m, 4H), 1.04−0.99 (m, 9H). ^{13}C NMR (100 MHz, $CDCl_3$) δ 171.25, 170.58, 170.36, 169.36, 169.16, 163.56, 161.70, 157.42, 156.81, 154.63, 153.00, 150.38, 148.70, 148.55, 133.26, 132.35, 131.74, 130.44, 130.14, 127.03, 125.27, 125.02, 122.22, 122.12, 116.95, 114.07, 113.06, 112.89, 96.32, 79.49, 77.40, 77.08, 76.77, 74.36, 70.91, 70.54, 70.50, 70.29, 69.78, 68.36, 68.04, 60.47, 58.98, 58.45, 57.55, 57.30, 56.66, 54.26, 53.38, 48.86, 39.13, 36.44, 35.79, 34.39, 29.74, 28.42, 26.42, 21.11, 18.48, 16.20, 14.25, 13.81, 13.71, 13.48, 13.38. LC−MS (ESI$^+$) m/z calcd for $C_{58}H_{74}Cl_2FN_{11}O_{11}S$ [M + H]$^+$, 1222.5, found 1224.3. HPLC t_R = 23.67 min (96% purity).

*4.1.11. (2S,4R)-N-(2-((14-(4-(4-(((6-(3-(2,6-Dichloro-3,5-dimethoxyphenyl)-1-methylureido)pyrimidin-4-yl)amino)phenyl)piperazin-1-yl)-3,6,9,12-tetraoxatetradecyl)oxy)-4-(4-methylthiazol-5-yl)-benzyl)-1-((S)-2-(1-fluorocyclopropane-1-carboxamido)-3,3-dimethylbutanoyl)-4-hydroxypyrrolidine-2-carboxamide (**LC-MF-7**).* **LC-MF-7** was synthesized in a similar manner as the bispecific compound **LC-MF-5**, white powder (29%). ^{1}H NMR (400 MHz, Chloroform-*d*) δ 8.70 (s, 1H), 8.13 (s, 1H), 7.48−7.32 (m, 1H), 7.20−7.09 (m, 3H), 7.04−6.88 (m, 4H), 6.55 (d, J = 5.0 Hz, 1H), 5.54 (s, 1H), 5.45 (s, 1H), 5.14 (s, 1H), 4.71−4.62 (m, 2H), 4.53−4.46 (m, 2H), 4.30−4.15 (m, 2H), 4.11−4.04 (m, 1H), 3.99−3.86 (m, 9H), 3.82−3.58 (m, 15H), 3.35−3.17 (m, 5H), 2.85−2.64 (m, 9H), 2.55 (s, 3H), 1.42−1.21 (m, 4H), 1.03−0.97 (m, 9H). ^{13}C NMR (100 MHz, $CDCl_3$) δ 170.55, 170.42, 169.35, 169.15, 163.62, 161.79, 157.58, 156.77, 154.63, 154.59, 152.96, 150.36, 148.75, 148.54, 133.20, 132.29, 131.75, 130.46, 129.91, 126.97, 125.24, 125.03, 122.17, 122.08, 116.91, 114.03, 113.99, 113.01, 112.87, 96.29, 79.50, 77.40, 77.08, 76.76, 74.35, 70.87, 70.57, 70.53, 70.49, 70.46, 70.32, 69.71, 68.51, 68.03, 58.95, 57.65, 57.27, 56.66, 54.19, 53.44, 48.97, 48.77, 39.14, 36.40, 35.82, 34.27, 29.74, 28.43, 26.41, 16.21, 13.80, 13.70, 13.51, 13.41. LC−MS (ESI$^+$) m/z calcd for $C_{60}H_{78}Cl_2FN_{11}O_{12}S$ [M + H]$^+$, 1266.5, found 1266.3. HPLC t_R = 23.64 min (98.3% purity).

*4.1.12. (2S,4R)-4-Hydroxy-N-(4-(4-methylthiazol-5-yl)benzyl)-pyrrolidine-2-carboxamide (compound **9**).* Step 1: Compound **8** (2.0 g, 8.3 mmol) and (2*S*,4*R*)-1-(*tert*-butoxycarbonyl)-4-hydroxypyrrolidine-2-carboxylic acid (1.92 g, 8.3 mmol) were dissolved in DCM (80 mL). HATU (3.3 g, 8.7 mmol) and Et_3N (4 mL, 29 mmol) were then added, and the mixture was stirred at room temperature

https://doi.org/10.1021/acs.jmedchem.5c00731
J. Med. Chem. 2025, 68, 13858−13871

overnight. The mixture was concentrated to dryness under reduced pressure to afford the crude product. The residue purified by silica gel chromatography (DCM/MeOH 50:1−20:1) to afford the product as a white oil (3.4 g)

Step 2: The product of the previous step was dissolved in 20 mL DCM, and HCl·EA (20 mL, 2 M) was gradually added under stirring. The reaction was stirred at room temperature for 2 h. The mixture was concentrated to dryness under reduced pressure to provide the title compound as a white solid (2.77 g, 7.8 mmol, 94%).

*4.1.13. (2S,4R)-1-((R)-2-Amino-3-methyl-3-(tritylthio)butanoyl)-4-hydroxy-N-(4-(4-methylthiazol-5-yl)benzyl)pyrrolidine-2-carboxamide (compound **10**).* Step 1: Compound **9** (71 mg, 0.2 mmol) and 2-((((9*H*-fluoren-9-yl)methoxy)carbonyl)amino)-3-methyl-3-(tritylthio)butanoic acid (123 mg, 0.2 mmol) were dissolved in 1.5 mL DMF. HATU (84 mg, 0.22 mmol) and Et_3N (100 μL, 0.7 mmol) were then added, and the mixture was stirred at 0 °C for 2 h. The reaction mixture was diluted with water (20 mL), extracted with EA (10 mL × 3), washed with brine (30 mL × 3). The combined organic layer was dried over anhydrous Na_2SO_4, filtered, and concentrated to dryness under reduced pressure to afford the crude product. The residue purified by silica gel chromatography (DCM/MeOH 60:1) to afford the product as a white solid (94 mg, 0.1 mmol, 50%).

Step 2: The product of the previous step was dissolved in 2 mL DCM, and then piperidine (400 μL) was added. The mixture was stirred at room temperature for 2 h. The mixture was concentrated to dryness under reduced pressure to provide the title compound as a yellow solid (54 mg, 0.078 mmol, 75%).

*4.1.14. (2S,4R)-1-((R)-2-(1-Fluorocyclopropane-1-carboxamido)-3-mercapto-3-methylbutanoyl)-4-hydroxy-N-(4-(4-methylthiazol-5-yl)benzyl)pyrrolidine-2-carboxamide (compound **11**).* Step 1: Compound **10** (490 mg, 0.71 mmol) and 1-fluorocyclopropane-1-carboxylic acid (74 mg, 0.71 mmol) were dissolved in 8 mL DMF. HATU (285 mg, 0.75 mmol) and Et_3N (300 μL, 2.1 mmol) were then added, and the mixture was stirred at room temperature for 4 h. The reaction mixture was diluted with water (100 mL), extracted with EA (20 mL × 3), washed with brine (50 mL × 3). The combined organic layer was dried over anhydrous Na_2SO_4, filtered, and concentrated to dryness under reduced pressure to afford the crude product. The residue purified by silica gel chromatography (DCM/MeOH 60:1) to afford the product as a yellow solid (520 mg, 0.66 mmol, 94%).

Step 2: The product of the previous step was dissolved in 8 mL DCM. Triisopropylsilane (4 mL) was then added followed by TFA (4 mL). The mixture was stirred at 0 °C for 0.5 h. The mixture was concentrated to dryness under reduced pressure to afford the crude product. The crude product purified by silica gel chromatography (DCM/MeOH 80:1) to provide the title compound as a purple solid (270 mg, 0.5 mmol, 75%).

*4.1.15. (2S,4R)-1-((R)-3-((2-(4-(4-((6-(3-(2,6-Dichloro-3,5-dimethoxyphenyl)-1-methylureido)pyrimidin-4-yl)amino)phenyl)piperazin-1-yl)ethyl)thio)-2-(1-fluorocyclopropane-1-carboxamido)-3-methylbutanoyl)-4-hydroxy-N-(4-(4-methylthiazol-5-yl)benzyl)pyrrolidine-2-carboxamide (**LC-CS-1**).* **LC-CS-1** was synthesized in a similar manner as the bispecific compound **LC-MF-1**, white powder (38%). ^{1}H NMR (400 MHz, Chloroform-*d*) δ 12.66 (s, 1H), 8.70 (s, 1H), 8.37 (s, 1H), 7.59−7.48 (m, 1H), 7.39 (t, *J* = 9.8 Hz, 3H), 7.31 (d, *J* = 8.7 Hz, 3H), 7.24 (d, *J* = 8.4 Hz, 2H), 6.96 (d, *J* = 8.5 Hz, 2H), 6.55 (s, 1H), 6.13 (s, 1H), 4.83−4.75 (m, 1H), 4.67−4.49 (m, 3H), 4.43−4.33 (m, 1H), 3.94 (s, 8H), 3.32 (s, 3H), 3.32−3.25 (m, 4H), 2.94−2.66 (m, 7H), 2.54 (s, 3H), 2.49−2.40 (m, 1H), 2.38−2.23 (m, 1H), 1.58−1.43 (m, 6H), 1.28 (s, 6H). ^{13}C NMR (100 MHz, $CDCl_3$) δ 171.31, 170.93, 170.72, 169.13, 163.03, 160.73, 155.90, 154.61, 153.48, 150.41, 148.93, 148.39, 138.31, 135.06, 131.81, 130.65, 129.80, 129.49, 127.45, 125.14, 117.12, 113.97, 95.90, 87.20, 79.32, 77.44, 77.12, 76.80, 69.80, 59.79, 57.61, 56.99, 56.72, 55.72, 52.98, 48.68, 47.47, 42.90, 37.85, 32.16, 31.99, 29.77, 29.43, 25.90, 25.80, 25.28, 22.77, 16.14. LC−MS (ESI$^+$) *m*/*z* calcd for $C_{51}H_{60}Cl_2FN_{11}O_7S_2$ [M + H]$^+$, 1092.4, found 1092.4. HPLC t_R = 25.48 min (95.75% purity).

*4.1.16. (2S,4R)-1-((R)-3-((3-(4-(4-((6-(3-(2,6-Dichloro-3,5-dimethoxyphenyl)-1-methylureido)pyrimidin-4-yl)amino)phenyl)piperazin-1-yl)propyl)thio)-2-(1-fluorocyclopropane-1-carboxamido)-3-methylbutanoyl)-4-hydroxy-N-(4-(4-methylthiazol-5-yl)benzyl)pyrrolidine-2-carboxamide (**LC-CS-2**).* **LC-CS-2** was synthesized in a similar manner as the bispecific compound **LC-MF-1**, white powder (43%). ^{1}H NMR (400 MHz, Chloroform-*d*) δ 12.58 (s, 1H), 8.59 (s, 1H), 8.26 (d, *J* = 0.9 Hz, 1H), 7.45 (t, *J* = 6.0 Hz, 1H), 7.35 (s, 1H), 7.33−7.26 (m, 2H), 7.25−7.17 (m, 3H), 7.15 (d, *J* = 8.8 Hz, 2H), 6.89−6.82 (m, 2H), 6.44 (s, 1H), 6.05−6.01 (m, 1H), 4.73−4.61 (m, 1H), 4.55−4.38 (m, 3H), 4.31−4.21 (m, 1H), 3.97−3.89 (m, 1H), 3.84 (s, 6H), 3.84−3.76 (m, 1H), 3.25−3.16 (m, 7H), 2.67 (s, 4H), 2.63−2.49 (m, 3H), 2.43 (s, 3H), 2.39−2.28 (m, 1H), 2.23−2.12 (m, 1H), 1.44 (s, 3H), 1.38 (s, 3H), 1.28−1.08 (m, 8H). ^{13}C NMR (101 MHz, $CDCl_3$) δ 170.18, 169.87, 169.67, 168.03, 161.94, 159.57, 154.83, 153.50, 152.39, 149.28, 147.28, 137.26, 133.96, 130.72, 129.51, 128.37, 126.30, 123.96, 116.00, 112.82, 94.74, 86.20, 78.21, 76.35, 76.03, 75.71, 68.56, 58.74, 55.95, 55.61, 51.85, 47.56, 46.20, 41.75, 36.84, 31.05, 28.67, 25.00, 24.82, 24.70, 15.06. LC−MS (ESI$^+$) *m*/*z* calcd for $C_{52}H_{62}Cl_2FN_{11}O_7S_2$ [M + H]$^+$, 1106.4, found 1106.4. HPLC t_R = 25.1 min (99.3% purity).

*4.1.17. (2S,4R)-1-((R)-3-((4-(4-(4-((6-(3-(2,6-Dichloro-3,5-dimethoxyphenyl)-1-methylureido)pyrimidin-4-yl)amino)phenyl)piperazin-1-yl)butyl)thio)-2-(1-fluorocyclopropane-1-carboxamido)-3-methylbutanoyl)-4-hydroxy-N-(4-(4-methylthiazol-5-yl)benzyl)pyrrolidine-2-carboxamide (**LC-CS-3**).* **LC-CS-3** was synthesized in a similar manner as the bispecific compound **LC-MF-1**, white powder (41%). ^{1}H NMR (400 MHz, Chloroform-*d*) δ 12.59 (s, 1H), 8.59 (s, 1H), 8.26 (s, 1H), 7.51−7.41 (m, 2H), 7.33−7.25 (m, 2H), 7.23−7.12 (m, 5H), 6.89−6.82 (m, 2H), 6.44 (s, 1H), 6.06−6.01 (m, 1H), 4.70−4.62 (m, 1H), 4.55−4.38 (m, 3H), 4.31−4.21 (m, 1H), 3.98−3.90 (m, 1H), 3.83 (s, 6H), 3.83−3.75 (m, 1H), 3.24−3.17 (m, 7H), 2.68 (s, 4H), 2.63−2.42 (m, 3H), 2.43 (s, 3H), 2.38−2.27 (m, 1H), 2.22−2.11 (m, 1H), 1.44 (s, 3H), 1.36 (s, 3H), 1.28−1.08 (m, 10H). ^{13}C NMR (101 MHz, $CDCl_3$) δ 170.24, 169.86, 169.65, 168.05, 161.92, 159.53, 153.50, 152.42, 149.29, 147.27, 137.28, 133.95, 130.74, 129.49, 128.37, 126.30, 123.86, 116.03, 112.80, 94.73, 78.20, 76.37, 76.05, 75.73, 68.45, 58.78, 56.14, 55.61, 51.81, 47.52, 45.91, 41.73, 36.90, 31.05, 28.67, 27.01, 25.88, 24.96, 24.56, 15.06, 13.13. LC−MS (ESI$^+$) *m*/*z* calcd for $C_{53}H_{64}Cl_2FN_{11}O_7S_2$ [M + H]$^+$, 1120.4, found 1120.4. HPLC t_R = 25.261 min (99.67% purity).

*4.1.18. (2S,4R)-1-((R)-3-((5-(4-(4-((6-(3-(2,6-Dichloro-3,5-dimethoxyphenyl)-1-methylureido)pyrimidin-4-yl)amino)phenyl)piperazin-1-yl)pentyl)thio)-2-(1-fluorocyclopropane-1-carboxamido)-3-methylbutanoyl)-4-hydroxy-N-(4-(4-methylthiazol-5-yl)benzyl)pyrrolidine-2-carboxamide (**LC-CS-4**).* **LC-CS-4** was synthesized in a similar manner as the bispecific compound **LC-MF-1**, white powder (45%). ^{1}H NMR (400 MHz, Chloroform-*d*) δ 12.68 (s, 1H), 8.69 (s, 1H), 8.36 (s, 1H), 7.75 (s, 1H), 7.60 (s, 1H), 7.39 (d, *J* = 7.8 Hz, 2H), 7.31 (s, 4H), 7.25 (s, 1H), 6.94 (d, *J* = 8.4 Hz, 2H), 6.53 (s, 1H), 6.15 (s, 1H), 4.76 (s, 1H), 4.61−4.47 (m, 3H), 4.35 (d, *J* = 15.8 Hz, 1H), 4.04 (s, 1H), 3.93 (s, 6H), 3.31 (s, 7H), 2.80 (s, 3H), 2.65−2.24 (m, 9H), 1.56−1.18 (m, 19H). ^{13}C NMR (101 MHz, $CDCl_3$) δ 170.18, 169.87, 169.67, 168.03, 161.94, 159.57, 154.83, 153.50, 152.39, 149.28, 147.28, 137.26, 133.96, 130.72, 129.51, 128.37, 126.30, 123.96, 115.98, 112.82, 94.74, 86.20, 78.21, 76.35, 76.03, 75.71, 68.56, 58.74, 55.95, 55.61, 51.85, 47.56, 46.20, 41.75, 36.84, 31.05, 28.67, 25.00, 24.82, 24.70, 14.88. LC-MS (ESI$^+$): calcd for $C_{54}H_{67}Cl_2FN_{11}O_7S_2$ [M + H]$^+$, 1134.40; found, 1134.5. HPLC t_R = 25.51 min (95.53% purity).

4.2. Cell Culture. KMS-11, RT112 and NCI-H1975 cell lines were cultured in RPMI 1640 medium supplemented with 10% fetal bovine serum (FBS) and 1% penicillin/streptomycin (P/S). HEK293 cells were grown in Dulbecco's modified Eagle's medium (DMEM) supplemented with 10% FBS and 1% P/S. MV-4-11 cells were cultured in Iscove's modified Dulbecco's medium (IMDM) supplemented with 10% FBS and 1% P/S.

4.3. Immunoblotting. KMS-11 cells were seeded into 24-well plates and cultured overnight before treatment with the compounds at various concentrations for the specified time. Cells were collected, washed with phosphate-buffered saline (PBS), and lysed in 2× loading buffer. The protein samples were subjected to SDS-PAGE gels and

https://doi.org/10.1021/acs.jmedchem.5c00731
J. Med. Chem. 2025, 68, 13858−13871

transferred to polyvinylidene difluoride (PVDF) membranes, followed by blocking with TBST containing 5% bovine serum albumin (BSA) for 1 h. The membranes were incubated with primary antibodies overnight at 4 °C. The antibodies used in our study were as follows: anti-FGFR1 (1:1000, Cat# 9740S), anti-FGFR2 (1:1000, Cat# 11835), anti-FGFR3 (1:1000, Cat# 4574S), anti-FGFR4 (1:1000, Cat# 8562S), anti-p-FGFR (Tyr653/654) (1:1000, Cat# 3471S), anti-p-ERK (T202/Y204) (1:2000, Cat# 4370T), anti-ERK (1:1000; Cat# 4695S), anti-p-FRS2-alpha (Y436) (1:1000, Cat# 3861S), anti-p-PLCγ1 (Y783) (1:1000, Cat# 2821S), anti-PLCγ1 (1:1000, Cat# 2822S), anti-p-AKT (S473) (1:2000, Cat# 4060S) and anti-AKT (1:2000, Cat# 9272S), were all purchased from Cell Signaling Technology. Anti-FRS2 [EPR14724] (1:1000, Cat# ab183492) was purchased from Abcam. Anti-PGC1a (1:5000, Cat# 66369-1-lg) was purchased from Proteintech. Anti-FGFR3 (1:1000, Cat# ET1703-65), anti-GAPDH (1:50000, Cat# ET1601-4) and antibeta actin (1:10000, Cat# R1207-1) were purchased from HUABIO. Anti-Flag-Tag (1:5000, Cat# T0053) was purchased from Affinity Biosciences.

4.4. Proteomics Analysis. To acquire TMT-labeled quantitative proteomic data, KMS-11 cells were initially seeded into 10 cm Petri dishes. Subsequently, the culture medium was supplemented with either 500 nM LC-MF-4 or blank control DMSO, followed by a 8 h incubation period. Each experiment was conducted in triplicate. Post-treatment, the medium was aspirated, and cells were harvested by centrifugation at 700 g and 4 °C. Comprehensive proteomic sequencing, including protein extraction, enzymatic digestion, TMT/iTRAQ labeling, HPLC fractionation, liquid chromatography-tandem mass spectrometry (LC-MS/MS), database interrogation, and bioinformatics analysis, was performed by Lianchuan Biotechnology (Hangzhou, China). Data visualization, including scatter plot generation, was performed using GraphPad Prism 8.

4.5. Molecular Modeling. Human crystal structures of FGFR3 (PDB code: 7DHL) and VHL (PDB code: 7PI4) were obtained from *Protein Data Bank*.[39,40] The *PROTAC-Model* method with default parameters was employed to predict the initial binding mode of the ternary complex of FGFR3-VHL-LC-MF-4 or LC-CS-4 as Weng et al. reported.[31] Subsequently, the ternary complex with the optimal docking score was subjected to 500 ns molecular dynamics (MD) simulations, following a protocol similar to previously reported studies.[41,42] During the 500 ns MD simulations, the time step was set to 2 fs and snapshots were recorded every 10 ps. The *CPPTRAJ* module in the *Amber 22* package was used to process the root-mean-square deviations (RMSDs).[43] 1,000 snapshots extracted from the 400 to 500 ns MD simulation trajectories were subjected to per-residue decomposition using the mechanics/generalized Born surface area (MM/GBSA) method.[44]

4.6. Immunofluorescence. To assess the FGFR3 degradation, KMS-11 cells were treated with 100 nM LC-MF-4 or LC-CS-4, fixed with 4% paraformaldehyde for 20 min, permeabilized with 0.3% Triton X-100 in PBS, and blocked with 1% w/v BSA in PBS at room temperature for 30 min. Subsequently, the cells were incubated with anti-FGFR3 antibody (Cat# 4574S, Cell Signaling Technology) overnight at 4 °C, followed by incubation with Alexa Fluor 488-conjugated secondary antibody (Cat# A0423, Beyotime Biotechnology) for 1 h and DAPI (Cat# C1002, Beyotime Biotechnology) for 5 min at room temperature in the dark. Cells were imaged using a Carl Zeiss LSM710 confocal fluorescence microscope.

4.7. Cell Viability Assay. The cell viability assay was performed using a luminescent ATP cell viability assay kit (Cat# K2401, APExBIO). Cells were seeded in 96-well plates and treated with the indicated doses of the compounds for 72 h. An equal volume of the luminescent ATP cell viability assay reagent was added and incubated at room temperature for 10 min before measuring the luminescence readings as relative light units (RLU). Cell viability rate (%) was calculated as follows: [(RLU compound − RLU blank)/(RLU control − RLU blank)] × 100.

4.8. RT-qPCR. Total RNA was isolated from RT112 cells using the TransZol Up Plus RNA Kit (Cat# ER501, TransGen Biotech), and the RNA concentration was determined using a NanoDrop 2000 spectrophotometer (Thermo Fisher Scientific). cDNA was synthesized using the HiScript III RT SuperMix for qPCR (+gDNA wiper) (Cat# R323-01, Vazyme) and gene expression levels were measured using the ChamQ Universal SYBR qPCR Master Mix (Cat# Q711-02, Vazyme), according to the manufacturer's protocol. RT-qPCR results were analyzed using the ΔΔCt method, with 18S as the housekeeping gene.

Human primers used for RT-qPCR was as follows:

UQCRC1 forward 5′-CACCGTGATGATGCTCTACC-3′ and reverse 5′CCACCACCATAAGTGCAGTC-3′;

POLRMT forward 5′-TATTCATGGTGAAGGATGCC-3′ and reverse 5′-TCTGTTCCAGACACCTTTCG-3′;

NDUFB4 forward 5′-TGCTTCAGTACAACGATCCC-3′ and reverse 5′-CACACAGAGCTCCCATGAGT-3′;

MRPL15 forward 5′-TGCTTCCACCAGAAGAACTG-3′ and reverse 5′-ACTTCCTGGCGAGTTCAAGT-3′;

PPARGC1A forward 5′-CTCACACCAAACCCACAGAG-3′ and reverse 5′-GTGTTGTGACTGCGACTGTG-3′;

18S forward 5′-CGCCGCTAGAGGTGAAATTC-3′ and reverse 5′-CTTTCGCTCTGGTCCGTCTT-3.

4.9. Colony Formation Assay. RT112 cells were plated in 35 mm plates and treated with DMSO or the test compounds at 37 °C for 14 days. The cells were then fixed with 4% paraformaldehyde for 10 min and stained with crystal violet for 10 min for observation.

4.10. ATP Assay. The cell cycle assay was performed using an ATP assay kit (Cat# S0027, Beyotime). The cells were lysed on ice after drug administration, and the relative light units (RLU) were measured. ATP content was calculated based on a standard curve.

4.11. Pharmacokinetic Study. Female C57BL/6 mice (19−22 g) employed in PK study were fasted for 8 h before drug administration. LC-MF-4 was dissolved in a vehicle containing 10% solution, 85% (10% HP-CD in saline), and 5% DMSO. Mice were administered LC-MF-4 solution intravenously (i.v.) at 5 mg/kg and p.o. at 20 mg/kg. Blood samples from each experimental mice were collected at 0.25, 0.5, 1, 2, 4, 6, 8, and 24 h (p.o.) or 0.083, 0.25, 0.5, 1, 2, 4, 8, and 24 h (i.v.) treatment. Plasma was harvested by centrifugation and analyzed by LC-QQQ/MS (64957C). Data acquisition was performed using the DAS 2.0.

4.12. Animal Study. Six-week-old female BALB/c nude mice were obtained from Charles River (Zhejiang, China). Ba/F3-FGFR3-TACC cells were subcutaneously injected into 6-week-old mice using Matrigel (082704; ABW). Once tumors reached an average volume of 150 mm^3, the mice were divided into three groups. The vehicle control, LC-MF-4, and LC-CS-4 (20 mg/kg) were administered orally once daily for 14 days, and the tumor size and body weight were measured three times a week. The study protocol was approved by the Institutional Animal Care and Use Committee (IACUC) of Precedo Pharmaceuticals Co., Ltd. (IACUC-20240408). During the study, the animal breeding and use were strictly conducted in accordance with the regulations of the International Management Committee for Assessment and Certification of Laboratory Animals.

4.13. Statistical Analysis. All data were collected from at least two independent replicate trials and are represented as the mean ± standard error of the mean (SEM). All data were analyzed using GraphPad Prism 8.0 software. Comparisons between two groups were performed using a two-tailed unpaired Student's *t* test, and comparisons among multiple groups were performed using a one-way analysis of variance (ANOVA) followed by Dunnett's post hoc test. Statistical significance was set at $p < 0.05$.

■ ASSOCIATED CONTENT

Supporting Information

The Supporting Information is available free of charge at https://pubs.acs.org/doi/10.1021/acs.jmedchem.5c00731.

Supplemental Figures S1−S5, Supplemental Tables S1−S4, NMR, and HPLC data (PDF)

Docking model of LC-MF-4 with FGFR3 and VHL from PDB entry 7DHL and 7PI4 (PDB)

Molecular formula strings (CSV)

https://doi.org/10.1021/acs.jmedchem.5c00731
J. Med. Chem. 2025, 68, 13858−13871

AUTHOR INFORMATION

Corresponding Authors

Lingfeng Chen − *School of Pharmacy, Hangzhou Medical College, Hangzhou 310014, China*; orcid.org/0000-0003-0089-6559; Phone: +86-571-88215622; Email: lfchen@hmc.edu.cn

Guang Liang − *School of Pharmacy, Hangzhou Medical College, Hangzhou 310014, China; Department of Pharmacy, Zhejiang Provincial People's Hospital, Affiliated People's Hospital, Hangzhou Medical College, Hangzhou 310014, China*; Phone: +86-577-86699396; Email: wzmcliangguang@163.com

Ping Huang − *School of Pharmacy, Hangzhou Medical College, Hangzhou 310014, China; Department of Pharmacy, Zhejiang Provincial People's Hospital, Affiliated People's Hospital, Hangzhou Medical College, Hangzhou 310014, China*; Email: huangpwly@sina.com

Di Ke − *Institute of Health and Medicine, Hefei Comprehensive National Science Center, Hefei 230601, China*; Email: kedi@ihm.ac.cn

Authors

Lulu Zheng − *School of Pharmacy, Hangzhou Medical College, Hangzhou 310014, China; Department of Pharmacy, Zhejiang Provincial People's Hospital, Affiliated People's Hospital, Hangzhou Medical College, Hangzhou 310014, China*

Jiaqi Cao − *School of Pharmacy, Hangzhou Medical College, Hangzhou 310014, China*

Lin Ma − *School of Pharmacy, Hangzhou Medical College, Hangzhou 310014, China*

Shiyan Chen − *School of Pharmacy, Hangzhou Medical College, Hangzhou 310014, China*

Xiansheng Cao − *School of Pharmacy, Hangzhou Medical College, Hangzhou 310014, China*

Ruixiang Luo − *School of Pharmacy, Hangzhou Medical College, Hangzhou 310014, China*

Yuhan Wang − *School of Pharmacy, Hangzhou Medical College, Hangzhou 310014, China*

Complete contact information is available at: https://pubs.acs.org/10.1021/acs.jmedchem.5c00731

Author Contributions

‖L.Z., J.C., L.M., and S.C. contributed equally to this work.

Notes

The authors declare no competing financial interest.

ACKNOWLEDGMENTS

This work was supported by the National Natural Science Foundation of China (82422068 to L.C.), the Natural Science Funding of Zhejiang Province (LDG25H300001 and LR24H300001 to L.C.), and the Zhejiang Medical and Health Science Project (2023KY622 to L.Z.).

ABBREVIATIONS

FBS, fetal bovine serum; FGFR3, fibroblast growth factor receptor 3; FRS2α, FGFR substrate 2 alpha; MD, molecular dynamics; MM/GBSA, mechanics/generalized Born surface area; PGC1α, peroxisome proliferator-activated receptor gamma coactivator 1-alpha; PK, pharmacokinetic; PLCγ, phospholipase C gamma 1; PROTAC, proteolysis-targeting chimera; RMSDs, root-mean-square deviations; RTKs, receptor tyrosine kinases; TACC3, transforming acidic coiled-coil containing protein 3; UC, urothelial carcinoma; VHL, von Hippel-Lindau

REFERENCES

(1) Beenken, A.; Mohammadi, M. The FGF family: biology, pathophysiology and therapy. *Nat. Rev. Drug Discovery* **2009**, *8* (3), 235−253.

(2) Katoh, M.; Nakagama, H. FGF receptors: cancer biology and therapeutics. *Med. Res. Rev.* **2014**, *34* (2), 280−300.

(3) Itoh, N.; Ornitz, D. Fibroblast growth factors: from molecular evolution to roles in development, metabolism and disease. *J. Biochem.* **2011**, *149* (2), 121−130.

(4) Eswarakumar, V. P.; Lax, I.; Schlessinger, J. Cellular signaling by fibroblast growth factor receptors. *Cytokine Growth Factor Rev.* **2005**, *16* (2), 139−149.

(5) Babina, I. S.; Turner, N. C. Advances and challenges in targeting FGFR signalling in cancer. *Nat. Rev. Cancer* **2017**, *17* (5), 318−332.

(6) Katoh, M. Therapeutics targeting FGF signaling network in human diseases. *Trends Pharmacol. Sci.* **2016**, *37* (12), 1081−1096.

(7) Chen, L.; Zhang, Y.; Yin, L.; Cai, B.; Huang, P.; Li, X.; Liang, G. Fibroblast growth factor receptor fusions in cancer: opportunities and challenges. *J. Exp. Clin. Cancer Res.* **2021**, *40* (1), 345.

(8) Chen, L.; Marsiglia, W. M.; Chen, H.; Katigbak, J.; Erdjument-Bromage, H.; Kemble, D. J.; Fu, L.; Ma, J.; Sun, G.; Zhang, Y.; et al. Molecular basis for receptor tyrosine kinase A-loop tyrosine transphosphorylation. *Nat. Chem. Biol.* **2020**, *16* (3), 267−277.

(9) Chen, L.; Fu, L.; Sun, J.; Huang, Z.; Fang, M.; Zinkle, A.; Liu, X.; Lu, J.; Pan, Z.; Wang, Y.; et al. Structural basis for FGF hormone signalling. *Nature* **2023**, *618* (7966), 862−870.

(10) Krook, M. A.; Reeser, J. W.; Ernst, G.; Barker, H.; Wilberding, M.; Li, G.; Chen, H. Z.; Roychowdhury, S. Fibroblast growth factor receptors in cancer: genetic alterations, diagnostics, therapeutic targets and mechanisms of resistance. *Br. J. Cancer* **2021**, *124* (5), 880−892.

(11) Facchinetti, F.; Hollebecque, A.; Bahleda, R.; Loriot, Y.; Olaussen, K. A.; Massard, C.; Friboulet, L. Facts and new hopes on selective FGFR inhibitors in solid tumors. *Clin. Cancer Res.* **2020**, *26* (4), 764−774.

(12) Singh, D.; Chan, J. M.; Zoppoli, P.; Niola, F.; Sullivan, R.; Castano, A.; Liu, E. M.; Reichel, J.; Porrati, P.; Pellegatta, S.; et al. Transforming fusions of FGFR and TACC genes in human glioblastoma. *Science* **2012**, *337* (6099), 1231−1235.

(13) Frattini, V.; Pagnotta, S. M.; Tala; Fan, J. J.; Russo, M. V.; Lee, S. B.; Garofano, L.; Zhang, J.; Shi, P.; Lewis, G.; et al. A metabolic function of FGFR3-TACC3 gene fusions in cancer. *Nature* **2018**, *553* (7687), 222−227.

(14) Loriot, Y.; Matsubara, N.; Park, S. H.; Huddart, R. A.; Burgess, E. F.; Houede, N.; Banek, S.; Guadalupi, V.; Ku, J. H.; Valderrama, B. P.; et al. Erdafitinib or chemotherapy in advanced or metastatic urothelial carcinoma. *N. Engl. J. Med.* **2023**, *389* (21), 1961−1971.

(15) Javle, M.; Lowery, M.; Shroff, R. T.; Weiss, K. H.; Springfeld, C.; Borad, M. J.; Ramanathan, R. K.; Goyal, L.; Sadeghi, S.; Macarulla, T.; et al. Phase II study of BGJ398 in patients with FGFR-altered advanced cholangiocarcinoma. *J. Clin. Oncol.* **2018**, *36* (3), 276−282.

(16) Goyal, L.; Shi, L.; Liu, L. Y.; Fece de la Cruz, F.; Lennerz, J. K.; Raghavan, S.; Leschiner, I.; Elagina, L.; Siravegna, G.; Ng, R. W. S.; et al. TAS-120 Overcomes Resistance to ATP-Competitive FGFR Inhibitors in Patients with FGFR2 Fusion-Positive Intrahepatic Cholangiocarcinoma. *Cancer Discovery* **2019**, *9* (8), 1064−1079.

(17) Katoh, M.; Loriot, Y.; Brandi, G.; Tavolari, S.; Wainberg, Z. A.; Katoh, M. FGFR-targeted therapeutics: clinical activity, mechanisms of resistance and new directions. *Nat. Rev. Clin. Oncol.* **2024**, *21* (4), 312−329.

(18) Goyal, L.; Saha, S. K.; Liu, L. Y.; Siravegna, G.; Leshchiner, I.; Ahronian, L. G.; Lennerz, J. K.; Vu, P.; Deshpande, V.; Kambadakone, A.; et al. Polyclonal secondary FGFR2 mutations drive acquired

resistance to FGFR inhibition in patients with FGFR2 fusion-positive cholangiocarcinoma. *Cancer Discovery* **2017**, *7* (3), 252−263.
(19) Saborowski, A.; Lehmann, U.; Vogel, A. FGFR inhibitors in cholangiocarcinoma: what's now and what's next? *Ther. Adv. Med. Oncol.* **2020**, *12*, 1758835920953293.
(20) Guercio, B. J.; Sarfaty, M.; Teo, M. Y.; Ratna, N.; Duzgol, C.; Funt, S. A.; Lee, C. H.; Aggen, D. H.; Regazzi, A. M.; Chen, Z.; et al. Clinical and genomic landscape of FGFR3-altered urothelial carcinoma and treatment outcomes with Erdafitinib: A Real-World Experience. *Clin. Cancer Res.* **2023**, *29* (22), 4586−4595.
(21) Facchinetti, F.; Hollebecque, A.; Braye, F.; Vasseur, D.; Pradat, Y.; Bahleda, R.; Pobel, C.; Bigot, L.; Deas, O.; Florez Arango, J. D.; et al. Resistance to selective FGFR inhibitors in FGFR-driven urothelial cancer. *Cancer Discovery* **2023**, *13* (9), 1998−2011.
(22) Sun, D.; Zhang, J.; Dong, G.; He, S.; Sheng, C. Blocking Non-enzymatic Functions by PROTAC-Mediated Targeted Protein Degradation. *J. Med. Chem.* **2022**, *65* (21), 14276−14288.
(23) Burslem, G. M.; Crews, C. M. Proteolysis-Targeting Chimeras as Therapeutics and Tools for Biological Discovery. *Cell* **2020**, *181* (1), 102−114.
(24) Chirnomas, D.; Hornberger, K. R.; Crews, C. M. Protein degraders enter the clinic - a new approach to cancer therapy. *Nat. Rev. Clin. Oncol.* **2023**, *20* (4), 265−278.
(25) Du, G.; Jiang, J.; Wu, Q.; Henning, N. J.; Donovan, K. A.; Yue, H.; Che, J.; Lu, W.; Fischer, E. S.; Bardeesy, N.; et al. Discovery of a Potent Degrader for Fibroblast Growth Factor Receptor 1/2. *Angew. Chem., Int. Ed.* **2021**, *60* (29), 15905−15911.
(26) Ma, L.; Li, Y.; Luo, R.; Wang, Y.; Cao, J.; Fu, W.; Qian, B.; Zheng, L.; Tang, L.; Lv, X.; et al. Discovery of a Selective and Orally Bioavailable FGFR2 Degrader for Treating Gastric Cancer. *J. Med. Chem.* **2023**, *66* (11), 7438−7453.
(27) Guo, L.; Liu, J.; Nie, X.; Wang, T.; Ma, Z. X.; Yin, D.; Tang, W. Development of selective FGFR1 degraders using a Rapid synthesis of proteolysis targeting Chimera (Rapid-TAC) platform. *Bioorg. Med. Chem. Lett.* **2022**, *75*, 128982.
(28) Hu, Z.; Zhang, Q.; Li, Z.; Yang, H.; Chen, X.; Zhang, Q.; Yang, T.; He, X.; Feng, Q.; He, J.; et al. Design, synthesis and antitumor activity of a novel FGFR2-selective degrader to overcome resistance of the FGFR2(V564F) gatekeeper mutation based on a pan-FGFR inhibitor. *Eur. J. Med. Chem.* **2024**, *275*, 116612.
(29) Kong, Y.; Zhao, X.; Wang, Z.; Yuan, S.; Chen, S.; Lou, S.; Ma, S.; Li, Y.; Wang, X.; Ge, Y.; et al. A Selective FGFR1/2 PROTAC Degrader with Antitumor Activity. *Mol. Cancer Ther.* **2024**, *23*, 1084−1094.
(30) Wang, Y. W.; Gao, Y. H.; Wang, C.; Zhang, P. F.; Wang, M.; Lan, L.; Liu, J. Y.; Shi, L.; Sun, L. P. Design, synthesis, and biological evaluation of novel FGFR1 PROTACs. *Bioorg. Chem.* **2025**, *155*, 108109.
(31) Weng, G.; Li, D.; Kang, Y.; Hou, T. Integrative Modeling of PROTAC-Mediated Ternary Complexes. *J. Med. Chem.* **2021**, *64* (21), 16271−16281.
(32) Hartl, I.; Brumovska, V.; Striedner, Y.; Yasari, A.; Schutz, G. J.; Sevcsik, E.; Tiemann-Boege, I. Measurement of FGFR3 signaling at the cell membrane via total internal reflection fluorescence microscopy to compare the activation of FGFR3 mutants. *J. Biol. Chem.* **2023**, *299* (2), 102832.
(33) Yang, Y.; Suhasini, A. N.; Jiang, Z.; Liu, N.; Rosconi, M.; Zhang, B.; Li, Y.; Dudgeon, D.; Seong, C.; Kim, S.; et al. A Tetravalent Bispecific Antibody Selectively Inhibits Diverse FGFR3 Oncogenic Variants. *Cancer Res.* **2024**, *84* (13), 2169−2180.
(34) Acquaviva, J.; He, S.; Zhang, C.; Jimenez, J. P.; Nagai, M.; Sang, J.; Sequeira, M.; Smith, D. L.; Ogawa, L. S.; Inoue, T.; et al. FGFR3 translocations in bladder cancer: differential sensitivity to HSP90 inhibition based on drug metabolism. *Mol. Cancer Res.* **2014**, *12* (7), 1042−1054.
(35) Luo, C.; Widlund, H. R.; Puigserver, P. PGC-1 Coactivators: Shepherding the Mitochondrial Biogenesis of Tumors. *Trends Cancer* **2016**, *2* (10), 619−631.
(36) Komura, K.; Hirosuna, K.; Tokushige, S.; Tsujino, T.; Nishimura, K.; Ishida, M.; Hayashi, T.; Ura, A.; Ohno, T.; Yamazaki, S.; et al. The Impact of FGFR3 Alterations on the Tumor Microenvironment and the Efficacy of Immune Checkpoint Inhibitors in Bladder Cancer. *Mol. Cancer* **2023**, *22* (1), 185.
(37) Bekes, M.; Langley, D. R.; Crews, C. M. PROTAC targeted protein degraders: the past is prologue. *Nat. Rev. Drug Discovery* **2022**, *21* (3), 181−200.
(38) Hudkins, R. L.; Allen, E.; Balcer, A.; Hoffman, I. D.; Iyer, S.; Neal, M.; Nelson, K. J.; Rideout, M.; Ye, Q.; Starrett, J. H.; et al. Discovery of TYRA-300: First Oral Selective FGFR3 Inhibitor for the Treatment of Urothelial Cancers and Achondroplasia. *J. Med. Chem.* **2024**, *67* (18), 16737−16756.
(39) Kuriwaki, I.; Kameda, M.; Iikubo, K.; Hisamichi, H.; Kawamoto, Y.; Kikuchi, S.; Moritomo, H.; Kondoh, Y.; Terasaka, T.; Amano, Y.; et al. Synthesis and structure-activity relationships of pyrimidine derivatives as potent and orally active FGFR3 inhibitors with both increased systemic exposure and enhanced in vitro potency. *Bioorg. Med. Chem.* **2021**, *33*, 116019.
(40) Law, R. P.; Nunes, J.; Chung, C. W.; Bantscheff, M.; Buda, K.; Dai, H.; Evans, J. P.; Flinders, A.; Klimaszewska, D.; Lewis, A. J.; et al. Discovery and Characterisation of Highly Cooperative FAK-Degrading PROTACs. *Angew. Chem., Int. Ed.* **2021**, *60* (43), 23327−23334.
(41) Fu, W.; Wang, E.; Ke, D.; Yang, H.; Chen, L.; Shao, J.; Hu, X.; Xu, L.; Liu, N.; Hou, T. Discovery of a Novel Fusarium Graminearum Mitogen-Activated Protein Kinase (FgGpmk1) Inhibitor for the Treatment of Fusarium Head Blight. *J. Med. Chem.* **2021**, *64* (18), 13841−13852.
(42) Fu, W.; Yang, H.; Hu, C.; Liao, J.; Gong, Z.; Zhang, M.; Yang, S.; Ye, S.; Lei, Y.; Sheng, R.; et al. Small-Molecule Inhibition of Androgen Receptor Dimerization as a Strategy against Prostate Cancer. *ACS Cent. Sci.* **2023**, *9* (4), 675−684.
(43) Roe, D. R.; Cheatham, T. E. 3rd. PTRAJ and CPPTRAJ: software for processing and analysis of molecular dynamics trajectory data. *J. Chem. Theory Comput.* **2013**, *9* (7), 3084−3095.
(44) Wang, E.; Sun, H.; Wang, J.; Wang, Z.; Liu, H.; Zhang, J. Z. H.; Hou, T. End-Point Binding Free Energy Calculation with MM/PBSA and MM/GBSA: Strategies and Applications in Drug Design. *Chem. Rev.* **2019**, *119* (16), 9478−9508.

https://doi.org/10.1021/acs.jmedchem.5c00731
J. Med. Chem. 2025, 68, 13858−13871